

Spectroscopy of New High Proper Motion Stars in the Northern Sky. I. New Nearby Stars, New High Velocity Stars, and an Enhanced Classification Scheme for M Dwarfs.

Sébastien Lépine^{1,2,3,4}, R. Michael Rich^{2,5} and Michael M. Shara¹

ABSTRACT

We define an enhanced spectral classification scheme for M dwarf stars, and use it to derive spectral classification of 104 northern stars with proper motions larger than $0.5'' \text{ yr}^{-1}$ which we discovered in a survey of high proper motion stars at low galactic latitudes. The final tally is as follows: 54 M dwarfs, 25 sdK and sdM subdwarfs, 14 esdK and esdM extreme subdwarfs, and 11 DA and DC white dwarfs. Among the most interesting cases, we find one star to be the coolest subdwarf ever reported (LSR2036+5059, with spectral type sdM7.5), a new M9.0 dwarf only about 6pc distant (LSR1835+3259), and a new M6.5 dwarf only 7pc from the Sun (LSR2124+4003). Spectroscopic distances suggests that 27 of the M dwarfs, 3 of the white dwarfs, and one of the subdwarfs (LSR2036+5059) are within 25pc of the Sun, making them excellent candidates for inclusion in the solar neighborhood census. Estimated sky-projected velocities suggest that most of our subdwarfs and extreme subdwarfs have halo kinematics. We find that several white dwarfs and non metal-poor M dwarfs also have kinematics consistent with the halo, and we briefly discuss their possible origin.

Subject headings: Solar Neighborhood — Stars: low-mass, brown dwarfs — Stars: subdwarfs — Stars: white dwarfs — Stars: kinematics

¹Department of Astrophysics, Division of Physical Sciences, American Museum of Natural History, Central Park West at 79th Street, New York, NY 10024, USA.

²Visiting Astronomer, Lick Observatory.

³Visiting Astronomer, MDM Observatory.

⁴Visiting Astronomer, KPNO.

⁵Department of Physics and Astronomy, University of California at Los Angeles, Los Angeles, CA 90095, USA.

1. Introduction

The current census of stars in the Solar Neighborhood (the volume of space within ≈ 25 pc of the sun) is believed to be significantly incomplete, especially at the faint end of the luminosity function. Despite the fact that increasing numbers of substellar objects (L dwarfs, T dwarfs), and low mass stars (M7-M9 dwarfs) are now being discovered with the help of large infrared surveys (Kirkpatrick *et al.* 1999; Delfosse *et al.* 1999; Gizis & Reid 1997) there remain significant numbers of red dwarfs and white dwarfs which are still unaccounted for (Henry *et al.* 1997).

Nearly all the local M dwarfs and white dwarfs are expected to be brighter than magnitude ~ 20 in the optical bands. The majority of them should be detectable as stars with large proper motions. If they haven't been identified yet it is because existing all-sky surveys of high proper motion stars (Luyten 1979, 1980) are themselves significantly incomplete (Scholz *et al.* 2000; Lepine, Shara, & Rich 2002b). Furthermore, the classification and characterization of even the known high proper motion stars is still under way (Gizis & Reid 1997; Jahreiss *et al.* 2001; Reid, Kilkenney, & Cruz 2002).

Recently, several new additions to the solar neighborhood have been confirmed from follow-up observations of newly discovered high proper motion stars (Phan-Bao *et al.* 2001; Henry *et al.* 2002; Scholz *et al.* 2002a; Reylé *et al.* 2002). Follow-up observations of faint stars with large proper motions have also revealed the existence of previously unreported types of objects like a very cool extreme subdwarf (Schweitzer *et al.* 1999), a magnetic DZ white dwarf (Reid, Liebert, & Schmidt 2001), and a pair of nearby cool white dwarfs (Scholz *et al.* 2002b).

In a previous paper (Lepine, Shara, & Rich 2002b) we have reported the discovery of 140 new stars with proper motions larger than $0.5'' \text{ yr}^{-1}$ at low galactic latitudes in the northern sky. For the past two years, we have been carrying out a large spectroscopic follow-up survey of the new high proper motion stars that we are finding in the northern sky. The spectroscopy is being performed at the Lick Observatory, the MDM Observatory, and the Kitt Peak National Observatory. This first paper of a series presents spectral classification of a first set of 104 stars, all of which are listed in Lepine, Shara, & Rich (2002b). Observations are described in §2. In §3, we describe our classification method, which expands on previous spectral index methods. Estimation of the radial velocities and calculation of the spectroscopic distances is detailed in §4, where we also discuss the kinematics of the objects. Especially interesting or intriguing stars are discussed in §5. Important results are briefly summarized in §6.

2. Spectroscopic observations

Spectra were obtained on six separate runs, at the Lick Observatory in August 2000, July 2001, and December 2001, at the MDM Observatory in February 2001, and May 2002, and at the Kitt Peak National Observatory in May 2002. All 64 Lick spectra were obtained with the KAST spectrograph, mounted at the Cassegrain focus of the 3m Shane Telescope. We imaged the stars through a 2.5" wide slit, onto the 600 l/mm grating blazed at 7500Å . The KAST camera uses a thinned CCD which displays significant fringing redwards of 7500Å , and special care was needed to account for the fringing (using extra dome flats), although some spectra appear to show residuals from the fringing pattern on the far red side. The instrument rotator was used to orient the slit vertically on the sky, to minimize slit loss due to atmospheric diffraction. Standard reduction was performed with IRAF, including sky subtraction, normalization, and removal of telluric lines. The calibration was done using a set of KPNO spectrophotometric standards (Massey *et al.* 1988; Massey & Gronwall 1990). The resulting spectra cover the range 6200-9000Å with a resolution of 2.34Å per pixel.

The first 34 MDM spectra (February 2001) were obtained with the Mark III Spectrograph mounted on the 2.4m Hiltner Telescope. Stars were imaged through a 1.5" slit, onto the 600 l/mm grating blazed at 5800Å . We used a thinned CCD camera (called "Echelle") which shows only slight fringing in the red. Standard reduction was performed with IRAF, including sky subtraction, normalization, and removal of telluric lines. For calibration, we used the same set of KPNO spectrophotometric standards that we used for the Lick observations (see above). The resulting spectra cover the range 5200-8800Å with a resolution of 2.55Å per pixel. Because of the lower sensitivity of the setup to light redwards of 8000Å , the spectra are very noisy beyond that limit. Because of variable conditions in some of the nights, removal of telluric lines was sometimes difficult, and residual telluric absorption remains in some of the spectra. On the second MDM run (May 2002) we used the MkIII Spectrograph again, but this time with the 300 l/mm grating blazed at 8000Å , which provided a clearer signal in the red. We also used a thick CCD ("Wilbur") to avoid problems with fringing. The 5 spectra from the second run cover the range 6000-9900Å with a resolution of 3.10Å per pixel.

Finally, we observed the very faint white dwarf LSR2050+7740 during a run on the Mayall 4m Telescope at the Kit Peak National Observatory. We used the RC Spectrograph with the LB1A camera. Stars were imaged through a 2.0" slit onto the 316 l/mm grating blazed at 7500Å (#BL181). The star was observed near the meridian with the slit oriented north-south to minimize slit loss due to atmospheric diffraction. Standard reduction was performed with IRAF, including sky subtraction, normalization with the KPNO spectrophotometric standards, and removal of telluric lines. The resulting spectrum covers the

range 5800-9100Å with a resolution of 1.74Å per pixel.

3. Spectral Classification

3.1. Spectral Indices and the Metallicity Scale

A well-defined spectral sequence for M dwarfs in the red part of the spectrum (6000Å-9000Å) was compiled by Kirkpatrick, Henry, & McCarthy (1991). This sequence has become the standard reference for the spectral classification of M dwarfs. Classification on this system is typically performed by fitting the spectrum of a star to this sequence, either by eye or numerically through minimization methods. However, since the work of Reid, Hawley, & Gizis (1995), spectral indices that measure the depth of various molecular bandheads are being used to provide a quantitative spectral classification of M dwarfs. Spectral indices have been defined, and their values calibrated against spectral type, by Reid, Hawley, & Gizis (1995) for classification of M dwarfs in the Palomar-MSU spectroscopic survey, by Kirkpatrick, Henry, & Simons (1995) for the classification of late-type M dwarfs, by Kirkpatrick *et al.* (1999) for the classification of late-type M dwarfs and L dwarfs, by Martín *et al.* (1999) also for the classification of late-type M dwarfs and L dwarfs, and by Hawley *et al.* (2002) for the classification of M dwarfs found in the Sloan Digitized Sky Survey. A total of 45 different spectral indices are defined in the 5 papers quoted above. All of them are correlated with spectral type, though some provide a better diagnosis than others.

A very useful classification scheme was developed by Gizis (1997, hereafter G97), based on four of the Reid, Hawley, & Gizis (1995) spectral indices (CaH1, CaH2, CaH3, TiO5). Several authors have performed spectral classification using this system (Gizis & Reid 1997; Schweitzer *et al.* 1999; Jahreiss *et al.* 2001; Cruz & Reid 2002). The G97 method separates red dwarfs into three metallicity classes: dwarfs (dM or M), subdwarfs (sdM), and extreme subdwarfs (esdM). It also yields a good spectral classification for sdM, esdM and early/intermediate M dwarfs, but is not appropriate for the classification of late-type M dwarfs because the four indices measure the strength of molecular features around 7000Å which tend to saturate beyond spectral type M6. Classification of late-type M dwarfs can be performed using the spectral indices defined in Kirkpatrick *et al.* (1999) and Martín *et al.* (1999), or by using the single index defined by Kirkpatrick, Henry, & Simons (1995). We maintain, however, that an improved and unified scheme for the quantitative classification of all M dwarfs is needed.

Here we expand on the G97 method, and define a set of spectral indices which measure most major features in the 6000Å-9000Å spectral range (see Table 2). In Figure 1, we

show the spectral features measured by each individual index. From G97, we adopt the CaH1, CaH2, CaH3 indices (which measure the strength of the CaH bands blueward of 7050Å) and the TiO5 index (which measures the TiO bandhead redward of 7050Å). From Hawley *et al.* (2002), we adopt the VO 7434 and TiO 8440 indices (renamed VO1 and TiO7, respectively) which measure the strength of the VO band redward of 7530Å and the TiO bandhead blueward of 8430Å. We introduce two new indices, TiO6 which measures the depth of the prominent TiO bandhead redward of 7600Å, and VO2, which measures the tail of that same TiO bandhead blended with the VO band feature redward of 7850Å which is very prominent in late-type M dwarfs. Our VO2 index is similar to the VO 7912 index defined in Hawley *et al.* (2002), but the reference level (denominator) is defined around 8140Å instead of 8410Å; we prefer to use a reference level that is closer on the spectrum to the measured feature. Finally, we define a new Color-M index which measures the slope of a pseudo-continuum using reference points defined in narrow spectral ranges with a local maximum in intensity. This color index is very useful in estimating the general shape of the spectral energy distribution.

The values of the spectral indices were calculated for all the stars using the SBANDS task in IRAF. Values obtained for all the M dwarfs, subdwarfs, and extreme subdwarfs (i.e. excluding all the white dwarfs), and listed in Table 3.

As a first step, we follow the prescription of G97 to separate our red dwarf stars into the three metallicity classes. We assume that all the stars in our list are gravitationally bound to the galaxy, which means they cannot have a transverse velocity larger than 500 km/s. Because our targets all have proper motions larger than 0.5 arcsec/yr, they must be within 200 pc of the sun, which means a distance modulus smaller than 6.5. Since all our stars have an apparent red magnitude larger than 12, this means none of our stars can have an absolute magnitude brighter than 5.5, and most are much fainter. This completely rules out the possibility that any of these stars are giants or supergiants.

The separation into M, sdM, and esdM classes is based on the ratio of the CaH band indices to the TiO5 index (see Figure 2). We use the relationships defined in G97 for the separation of the stars into the different classes; these relationships are illustrated on Figure 2. To be considered an sdM/esdM, a star has to be within the limits defined by G97 in at least two of the diagrams. The low value of the CaH1 index for three late-type M dwarfs ($\text{TiO5} < 0.35$) results from a low signal-to-noise ratio in those stars around where CaH1 is measured. The CaH2/TiO 5 relationship was used to separate the esdM from the sdM. For the late K dwarfs and early M dwarfs, the G97 molecular bands criteria are more ambiguous; the CaH indices and the TiO5 index all converge to 1 toward earlier spectral types. There appear to be a number of stars with $\text{TiO5} > 0.7$ that could be M dwarfs. However, these would

have a spectral type earlier than M2, which means they would have an absolute magnitude $M_R < 8$. However, if they are M dwarfs they would be too faint ($R > 14$) to be within a few hundred parsecs. Because of their large proper motions ($\mu > 0.5'' \text{ yr}^{-1}$) these M dwarfs would have extremely large transverse velocities ($V_T > 500 \text{ km s}^{-1}$). For these reasons, it is likely that these stars are relatively nearby subdwarfs, instead of very distant, very high-velocity dwarfs.

3.2. M dwarfs

Our spectral types for the M dwarfs are assigned based on our expanded classification scheme which uses all the indices defined in Table 2. We have kept the relationships defined by G97 for the CaH2, CaH3, and TiO5 indices. The spectral type S_P correlates with these indices as:

$$S_P = 7.91 \text{ CaH2}^2 - 20.63 \text{ CaH2} + 10.71 \quad (\text{M0} - \text{M6}) \quad (1)$$

$$S_P = -18.00 \text{ CaH3} + 15.80 \quad (\text{M0} - \text{M6}) \quad (2)$$

$$S_P = -9.64 \text{ TiO5} + 7.76 \quad (\text{M0} - \text{M6}) \quad (3)$$

We give in parentheses the range over which these relationships are valid. There are weaknesses to these indices which we now note, as a prelude to an improved classification system given below. First, the three indices above do not make use of the full spectral range 6000Å-9000Å where several strong molecular bands are found in M dwarfs. Second, the CaH2, CaH3 and TiO5 indices are defined in a low-intensity region of the optical spectral energy distribution (for intermediate and late-type dwarfs). A third problem is that they are not strictly independent, since CaH2, CaH3, and TiO5 all use the same pseudo-continuum region as their reference point (7042Å-7046Å). This reference region is only 4Å wide, and is therefore sensitive to spectral noise; any significant instrumental deviation in the 7042Å-7046Å region propagates equally in all three indices.

To derive the correlations for the other indices, we first obtained a crude spectral typing by visual inspection of the spectra and comparison with the Kirkpatrick, Henry, & McCarthy (1991) sequence. We then made fine corrections to the spectral types (typically by no more than one subtype), until we obtained a clean sequence where all indices were linearly correlated with spectral type. The final sequence is shown in Figure 3. The few outlying points in the graphs are associated with stars for which we only have a noisy spectrum (especially LSR0212+7012, LSR0200+5530, and LSR0646+3412). We used linear regressions to obtain the following relationships:

$$S_P = -30.5 \text{ VO1} + 32.2 \quad (\text{M2} - \text{M8}) \quad (4)$$

$$S_P = -11.2 \text{ TiO6} + 11.9 \quad (\text{M2} - \text{M8}) \quad (5)$$

$$S_P = -10.5 \text{ VO2} + 12.4 \quad (\text{M3} - \text{M9}) \quad (6)$$

$$S_P = -11.0 \text{ TiO7} + 13.7 \quad (\text{M3} - \text{M9}) \quad (7)$$

Again we give in parentheses the range over which each of the relationships is valid. The VO1, TiO6, VO2, and TiO7 relationships are valid for later spectral types than are the CaH2, CaH3, and TiO5 relationships. The indices, taken together, can be used to obtain spectral types over the whole M dwarf range to an accuracy of about half a spectral type.

While the variation of all the spectral indices with spectral type appears to be linear, there appears to be an exponential progression of the Color-M index over the M dwarf sequence. In Figure 3, we plot the logarithm of the Color-M index, and show that it can be fitted with a linear relationship in the M3-M8 range. The Color-M uses two spectral regions separated by more than 1500\AA and is thus not as reliable as the other indices for spectral classification purposes, as it is more sensitive to slit loss, extinction, and other calibration errors. Nevertheless, the correlation is reasonably good, and the Color-M index may be used to help determine the spectral type of intermediate M dwarfs (M4-M8) using the relation:

$$S_p = 7.5 \log(\text{Color} - \text{M}) + 1.6 \quad (\text{M4} - \text{M8}) \quad (8)$$

The complete sequence of M dwarf spectra is displayed in Figures 4-5. One can verify that there is a smooth, continuous evolution toward later types.

We further examined the spectra for any indication of $H\alpha$ ($\lambda 6563$) in emission. Given the quality and resolution of the spectra, we determined that $H\alpha$ detection could be considered significant if it had an equivalent width smaller than about -2.0\AA . We added the subscript e to stars which qualified as $H\alpha$ emitters under this criterion. Close observation of the spectra suggests that several more stars (including all those of spectral type 6.0 and later) may also be $H\alpha$ emitters, but the equivalent width of the $H\alpha$ line was too weak to be considered significant under the criterion above. High resolution observations of the spectral region around 6563\AA would be required in order to determine which stars can be considered to be emission-line stars in a broader sense. It is remarkable that we find only 8 emission-line stars in our sample of 54 M dwarfs, especially given the large number of M5-M6 stars in the sample. Generally, about half of the M5-M6 dwarfs are found to be active (Gizis *et al.* 2000). Because activity is correlated with age, this possibly indicates that most stars in our sample are relatively old M dwarfs. This would be consistent with the relatively larger velocities that we find for most of them (see §4.4 below).

3.3. Subdwarfs and extreme subdwarfs

For sdM stars, we simply follow the G97 classification system, which uses only the CaH2 and CaH3 indices:

$$S_P = 7.91 \text{ CaH2}^2 - 20.63 \text{ CaH2} + 10.71 \quad (\text{sdK5} - \text{sdM7}) \quad (9)$$

$$S_P = -16.02 \text{ CaH3} + 13.78 \quad (\text{sdK5} - \text{sdM7}) \quad (10)$$

In this system, negative values of S_P correspond to sdK stars, with $S_P = -2 \rightarrow \text{sdK5}$, and $S_P = -1 \rightarrow \text{sdK7}$. We plot the distribution of CaH1, CaH2, and CaH3 values as a function of the sdM subtype in Figure 6. Because the TiO and VO bands are very weak in subdwarfs, they cannot be used as classification criteria. The Color-M term again appears to increase exponentially with the subtype, loosely following the relationship:

$$S_p = 7.3 \log(\text{Color} - M) - 0.6 \quad (11)$$

As expected, the slope of the pseudo-continuum measured by Color-M is significantly shallower for a given subtype than it is for the M dwarfs. The complete sequence of sdM spectra is displayed in Figure 7. One of our subdwarfs is classified with a very late spectral type sdM7.5. To the best of our knowledge, this is the coolest subdwarf ever identified.

For esdM stars, we also use the G97 calibration based on the CaH2 and CaH3 indices.

$$S_P = 7.91 \text{ CaH2}^2 - 20.63 \text{ CaH2} + 10.71 \quad (\text{esdK5} - \text{sdM7}) \quad (12)$$

$$S_P = -13.47 \text{ CaH3} + 11.50 \quad (\text{esdK5} - \text{sdM7}) \quad (13)$$

Again, negative values of S_P here correspond to esdK stars, with $S_P = -2 \rightarrow \text{esdK5}$, and $S_P = -1 \rightarrow \text{esdK7}$. We plot the distribution of CaH1, CaH2, and CaH3 values as a function of the sdM subtype in Figure 8. The Color-M term is again correlated with spectral type, following approximately the relationship:

$$S_p = 22.0 \log(\text{Color} - M) - 4.1 \quad (14)$$

Many of our esdM spectra (especially those from the 2001 MDM run) are relatively noisy in the red beyond 8000\AA . For this reason, the Color-M index is not very reliable for those stars. The 3 points in the bottom panel of Figure 8 that lie well outside the relation defined in equation 14 are from noisy MDM spectra. We suspect that the correlation between the esdM subtype and the Color-M index is actually very well defined. Spectra obtained with minimal slit loss and which are carefully normalized are, of course, required if the Color-M index is to be used for the classification of esdM stars. The complete sequence of esdM spectra is displayed in Figure 9.

3.4. White Dwarfs

The white dwarf stars in our sample are easily identified because they show none of the molecular features observed in the red dwarf stars. We compared our spectra to the catalog compiled by Wesemael (1993), and examined the spectra for the presence of $H\alpha$ in absorption. The 11 white dwarfs in our sample are either completely featureless (DC stars) or display some weak $H\alpha$ emission (cool DA stars).

Following the definition that the numerical spectral subtype of white dwarfs follows $50,400/T_{eff}$, we perform blackbody fits to our white dwarf spectra in the 6000-9000Å range. The corresponding blackbody temperatures are given in Table 3. The fits are accurate to $\pm 250\text{K}$, and the spectral typing is accurate to one spectral subtype. All the stars in our sample are late-type DA or DC white dwarfs, with DC7 being the earliest, and DC10 the latest. Our spectra for the white dwarf stars are plotted in Figure 10. Because we used observational setups optimized for the observation of red dwarf stars, our white dwarf spectra are sometimes very noisy, and the classification is not very reliable. The assignment of white dwarfs in the DC class is particularly dubious, and may simply result from our inability to detect the $H\alpha$ absorption line in noisy spectra. Still, our spectra clearly show that all the white dwarfs discovered in the sample are relatively cool, probably old objects.

4. Distances and kinematics

4.1. Reduced proper motion diagrams

A most useful tool for pre-selecting classes of high proper motion stars is the reduced proper motion diagram. Recently, Salim & Gould (2002) have demonstrated that dwarfs, subdwarfs, and white dwarfs can be separated out when the ratio of infra-red to optical colors is used in making the reduced proper motion diagrams. The reduced proper motion H is obtained by adding the logarithm of the proper motion to the apparent magnitude of the star (Luyten 1925). Here we use two different reduced proper motion terms:

$$H_R \equiv R + 5 + 5 \log \mu = M_R + 5 \log v_t - 3.38 \quad (15)$$

$$H_{K_s} \equiv K_s + 5 + 5 \log \mu = M_{K_s} + 5 \log v_t - 3.38 \quad (16)$$

Because both the apparent magnitude (R , K_s) and proper motion (μ) are a function of the distance to the star, the distance terms cancel, and so the reduced proper motion really is a measure of the combined absolute magnitude (M_R , M_{K_s}) and transverse velocity (v_t). Reduced proper motion diagrams are plots of the reduced proper motion against a color term.

We have made reduced proper motion diagrams using $[M_R, B-R]$ and $[M_{K_s}, R-K_s]$. In Figure 11, we plot the stars for which the corresponding magnitudes are available, using different symbols for the different classes of objects: filled circles for M dwarfs, open squares for sdM, filled triangles for esdM, and asterisks for the white dwarfs. On the $[M_R, B-R]$ diagram, white dwarfs populate a distinct locus, but it is not possible to distinguish the dwarfs from the subdwarfs. On the $[M_{K_s}, R-K_s]$ diagram however, the dwarfs, subdwarfs, and white dwarfs clearly occupy different loci. Proper motion and optical+infrared photometry alone can thus be used to guess what class of object one is dealing with, although spectroscopic confirmation is still required for certainty. This however, is a very useful method for pre-selecting stellar populations for follow-up observations.

4.2. Spectroscopic distance estimates

To obtain a calibration of the absolute magnitude against spectral type for M dwarfs, we used a set of nearby stars for which there exist parallax measurements accurate to better than 10%. We selected 55 stars from the NStars database (<http://nstars.arc.nasa.gov>) spanning a range of spectral types from M0.5 V to M8.0 V. There were very few objects in the M7.0 to M9.0 range, so we complemented the sample with 11 late-type dwarfs ranging from M6.5 V to M9.5 V whose parallaxes are given in Dahn *et al.* (2002). We proceeded to recover the B, R, and K_s magnitudes of those stars *using the same sources as those used for our sample of new high proper motion stars*, namely the Guide Star Catalog-II (GSC2.2.1) for the B and R magnitudes, and the 2MASS Second Incremental Release for the K_s magnitude. This procedure guarantees that the stars can then be compared on exactly the same magnitude system. While not all the stars had counterparts in the GSC2.2.1 or 2MASS, we did obtain reference magnitudes for at least 35 stars in each band. We then used the parallax measurements to derive a spectral-type / absolute magnitude calibration.

The correlations between spectral type and absolute magnitudes are shown in Figure 12. the relationship is clearly not linear across the M dwarf sequence, as the absolute B and R magnitudes drop quickly between spectral types M4 and M6; the absolute K magnitude also appears to drop faster between M3 and M5. We found that the overall behavior of the correlations could be modeled using third order polynomials. We performed χ^2 minimization fits to obtain the following empirical relationships between spectral types (S_P) and absolute magnitudes:

$$S_P(M) = 0.0156 M_B^3 - 0.730 M_B^2 + 11.8 M_B - 60.4 \quad (17)$$

$$S_P(M) = 0.0143 M_R^3 - 0.531 M_R^2 + 7.02 M_R - 28.1 \quad (18)$$

$$S_P(M) = 0.0974 M_{K_s}^3 - 2.076 M_{K_s}^2 + 15.4 M_{K_s} - 35.9. \quad (19)$$

We then used equations 17-19 to derive reference absolute magnitudes for each given spectral type S_P , and used these to obtain a spectroscopic distance estimate for each of our M dwarfs. Results are listed in Table 4. For stars with magnitudes in more than one band, the average distance is used; distance estimates in the different bands usually agreed to better than 30%.

We use the same method to determine a spectral-type / absolute magnitude calibration for sdM and esdM stars. We used as reference a set of 25 sdM and 19 esdM stars with spectral type and astrometric parallax given in G97. We looked for counterparts of these stars in the Guide Star Catalog-II (GSC2.2.1), and the 2MASS Second Incremental Release. The empirical spectral-type / absolute magnitude relationships are plotted in Figures 13-14. In all cases, the relationships appear to be linear. We thus performed χ^2 minimization fit of first order polynomials to obtain the following empirical relationships between spectral types (S_P) and absolute magnitudes. For the subdwarfs (sdM), we find:

$$S_P(\text{sdM}) = 1.12 M_B - 12.4 \quad (20)$$

$$S_P(\text{sdM}) = 1.13 M_R - 10.0 \quad (21)$$

$$S_P(\text{sdM}) = 1.65 M_{K_s} - 10.4. \quad (22)$$

And for the extreme subdwarfs (esdM), we find:

$$S_P(\text{esdM}) = 1.85 M_B - 23.2 \quad (23)$$

$$S_P(\text{esdM}) = 2.05 M_R - 21.4 \quad (24)$$

$$S_P(\text{esdM}) = 2.68 M_{K_s} - 21.6. \quad (25)$$

Distances for the sdM and esdM stars in our sample are based on these empirical relationships. Estimated values are given in Table 4.

Errors on the distance estimates depend on three main factors. First of all, there is an uncertainty related to the scatter in the spectral-type/absolute magnitude relationships. This scatter arises because of errors in the magnitudes and/or astrometric parallax, but may also result from an intrinsic scatter in the empirical relationship. There is typically a 0.5 magnitude scatter in the spectral-type/absolute magnitude relationship which translates into a distance error of about 25%. Furthermore, there is also an error of about 0.5 mags in the POSS-II photographic B and R magnitudes, which should also result in an extra 25% error on the distance estimate. The error is much smaller for the 2MASS K_s magnitude, but we do not have K_s values for all the stars. The fact that we use a combination of the spectral-type/absolute magnitude relationships for the B , R and K_s somehow reduces the errors on the distance estimate. Nevertheless, there should be a basic uncertainty on all the distances of M dwarfs and subdwarfs of about 35%.

Second, there is a significant difference between the calibrations of the different metallicity classes. This is especially true for early type stars, where for example an M0V star is fully 3 magnitudes brighter in the B and R bands than an esdM0 (see Figs. 12-14). While it is easy to distinguish dwarfs and extreme subdwarfs, the separation between dwarfs and subdwarfs, and between subdwarfs and extreme subdwarfs is arbitrary, and one actually expects to find a continuous distribution of stars over the whole metallicity range. The rough separation into only three metallicity classes thus introduces errors in the distance estimates. A star lying at the limit between two spectral classes can fall up to one magnitude from one or another spectral-type/absolute magnitude relationship, which means its distance estimate could be up to 60% in error.

A third factor is the possibility that some of the stars are actually unresolved binaries. Distances of unresolved binaries tend to be underestimated as the pair is intrinsically brighter for its apparent spectral type. The effect is largest for two M dwarfs of equal luminosity (and mass), where the apparent distance is underestimated by a factor $\sqrt{2}$, or about 40%.

Distance estimates for M dwarfs should be relatively more accurate than for the subdwarfs and extreme subdwarfs. The M dwarfs are better defined as a class, and their spectral-type/absolute magnitude relationship is supported by a larger number of astrometric standards (67 stars). Our relationships for sdM and esdM stars, on the other hand, are derived using fewer astrometric standards (25 stars for the sdM, and only 19 for the esdM). All things considered, our distance estimates *for individual objects* are probably accurate to about 50% for the M dwarfs, and to a factor of two for the sdM and esdM.

For the white dwarfs, we obtain very crude photometric distances with the B-R color, by using the relation given in Oppenheimer *et al.* (2001):

$$M_B = 12.73 + 2.58(B - R). \quad (26)$$

For those stars for which we do not have B magnitudes, we compare them with other white dwarfs in our sample with similar spectral types and estimated their relative distances based on their relative R magnitudes. Photometric distances for the white dwarfs are listed in Table 1. The accuracy of the distance estimates is very dependent on the accuracy of the $B - R$ color term. Because we use photographic B and R magnitudes, large errors (possibly up to a factor of 2) can be expected in the distance measurements.

4.3. Radial velocities

Our medium resolution (2-3Å per pixel) spectra were initially obtained for the purpose of classification alone, and are not ideally suited for measuring radial velocities. Nevertheless,

we find that radial velocities can still be obtained with typical errors of $\pm 30 - 50 \text{ km s}^{-1}$. While relatively large, these errors are nevertheless reasonably small when one deals with old disk or halo stars, which can have radial velocities of a few hundred km s^{-1} . Because our sample of high proper motion stars is strongly biased towards stars with very large velocity components, we naturally expect many of the stars to also have very large radial velocities.

We estimate radial velocities for each of our red dwarfs and subdwarfs by measuring the centroids of strong atomic absorption lines. In subdwarfs and extreme subdwarfs, we use two different sets of lines depending on the available wavelength coverage. For the 2001 MDM spectra, more sensitive at shorter wavelengths, we use the Na I $\lambda 5889.9$ and $\lambda 5895.9$ doublet and the Ca I $\lambda 6122.2$ and $\lambda 6162.7$ lines. For the Lick spectra and the 2002 MDM spectra, more sensitive at longer wavelengths, we use the K I $\lambda 7664.9$ and $\lambda 7699.0$ lines and the Ca II $\lambda 8542.1$ and $\lambda 8662.1$ lines. For the M dwarfs, all radial velocity measurements are based mainly on the centroids of the K I $\lambda 7664.9$ and $\lambda 7699.0$ lines. In emission line stars, we also measured the centroid of the $H\alpha$ emission line. It was not possible to obtain radial velocities from the featureless DC white dwarfs and for 2 of the DAs with very weak and noisy $H\alpha$ lines. However, we have obtained radial velocity estimates for 3 DA white dwarfs, by measuring the centroid of the core of the $H\alpha$ absorption.

For all the stars in the MDM runs, we measured the wavelength shifts relative to the XeNeAr comparison arcs obtained after each exposure. For the Lick spectra, sky lines from each individual exposure were used as a reference. Heliocentric radial velocities (HRV) were calculated after applying the relevant corrections. The resulting values are listed in Table 1.

4.4. Kinematics

We derive UVW components of the space velocity for each individual object using the proper motion, spectroscopic distance estimate, and radial velocity. We take the U component to be the velocity toward the galactic center, V the velocity toward the direction of galactic rotation, and W the velocity toward the north galactic pole, all calculated relative to the local standard of rest (l.s.r.). We use for the motion of the Sun relative to the l.s.r. the empirically estimated values $[U, V, W] = [+10, +5, +7] \text{ km s}^{-1}$ (Dehnen & Binney 1998). We plot the distribution in the VU, VW and UW planes in Figure 15 for the M dwarfs, in Figure 16 for the white dwarfs, and in Figure 17 for the subdwarfs and extreme subdwarfs.

The velocity distribution of the different classes of objects are compared to the observed distribution of local weakly metal-poor and strongly metal-poor stars (Chiba & Beers 2000). The dotted lines in Figs.15-17 mark the observed 2σ dispersion of a large sample of solar

neighborhood stars with $[\text{Fe}/\text{H}] \simeq -0.5$, which are associated with the galactic disk. Based on Chiba & Beers (2000), we hence adopt a velocity space distribution for disk stars centered on $[U, V, W] = [0, -30, 0] \text{ km s}^{-1}$, with a dispersion $[2\sigma_U, 2\sigma_V, 2\sigma_W] = [100, 110, 60] \text{ km s}^{-1}$. The dashed lines in Figs.15-17 mark the observed 2σ distribution of $[\text{Fe}/\text{H}] \simeq -2.5$ stars, and associated with the galactic halo. For halo stars, we adopt a velocity space distribution centered on $[U, V, W] = [0, -190, 0] \text{ km s}^{-1}$, with a dispersion $[2\sigma_U, 2\sigma_V, 2\sigma_W] = [280, 220, 190] \text{ km s}^{-1}$, again based on the distribution of very metal-poor stars reported by Chiba & Beers (2000).

The observed distribution in UVW velocity space for our M dwarfs (Fig.15) shows a relatively large scatter, significantly larger than expected for non-metal poor disk stars. Assuming that non-metal poor M dwarfs should have the same kinematics as more massive stars, over 95% of the local M dwarfs are expected to fall within the 2σ range illustrated in Fig.15. We find, however that about 40% of our stars fall outside that range. Two major effects possibly compound to yield the large velocity dispersion of our sample. First, the errors on the individual UVW components are relatively large, since they depend on the spectroscopic distance measurements and radial velocities, both of which have relatively large uncertainties. It is possible that more accurate measurements would yield a smaller scatter in the velocity distribution. Second, and most important, these stars have been selected based on their having large proper motions, which means that our sample is strongly biased in favor of stars with unusually large velocities.

Even if we account for the relatively large errors in the UVW estimates, our sample clearly contains a significant number of M dwarfs whose kinematics is more consistent with a halo membership (see Fig.15). Hence we conclude that without a doubt *there exist non metal-poor M dwarf stars with halo-like kinematics around the neighborhood of the Sun*. Since it is unlikely that these stars were actually born in the halo, there must be a mechanism that is responsible for sending disk stars into halo-like orbits. Dynamical ejection during promiscuous encounters of binary and single stars in star clusters is one possibility (Hurley & Shara 2002), although these are arguably relatively rare events. These low-mass, non metal-poor stars with unusually large velocities could also have originated in very massive star clusters, where the rapid expulsion of cluster gas by massive stars can result in the evaporation from the cluster of less massive members (Kroupa 2002). Alternatively, these stars could have been accreted from a satellite galaxy in a merger event with the Milky Way. Another possibility is that these stars are actually bulge stars that have been sent into very elliptical orbits through gravitational perturbations in dense regions of the bulge (Raboud *et al.* 1998). Our current sample of M dwarfs with halo-like kinematics is however relatively small at this point. Clearly, follow-up observations of more faint high proper motion stars are required to discover more of the non-metal poor, high velocity stars, and better characterize their group kinematics.

Two of the stars in our sample of M dwarfs have extremely large velocity components which place them well outside the 2σ limit of very metal-poor (halo) stars. These are LSR1844+0947 (M2.0V) and LSR2010+3938 (M1.5V). These happen to be the two earliest stars in our sample of M dwarfs. To find non-metal poor stars with such unbelievably large velocities raises suspicions about their estimated distances and radial velocities. In particular, those stars could be misclassified subdwarfs, in which case they could be much closer and their velocities would then fall within the normal range of metal-poor stars. We indicate this possibility by labeling LSR1844+0947 as (sd)M2.0V, and LSR2010+3938 as (sd)M1.5V. In Table 4, we give in parenthesis the estimated distances and velocity components for both stars under the assumption that they are subdwarfs.

The velocity space distribution of our 11 white dwarfs is plotted in Figure 16. Though we have very few objects, and the errors on the distances (and thus on the velocity components) are relatively large, it does appear that the white dwarfs have a velocity space distribution that is very similar to that of our M dwarfs, with most of them falling within or just outside the limits of disk stars, and a few outliers with halo-like kinematics. While it is tempting to argue that the white dwarfs with the largest space velocities are actually members of the population of old halo white dwarfs claimed by Oppenheimer *et al.* (2001), it is not possible at this point to exclude the possibility that the high velocity white dwarfs are drawn from the same population as those high velocity, non metal-poor M dwarfs. If so, these white dwarfs would not have been born with halo kinematics, rather acquiring them through some dynamical mechanism, conceivably the one that put large numbers of non metal-poor M dwarfs on halo-like orbits (see above).

The velocity space distribution of our subdwarfs and extreme subdwarfs (Fig.17), on the other hand, is largely consistent with a population of true halo stars. A significant number of stars are found outside the 2σ limits of the very metal poor stars. This again may be due to the large errors in our velocity estimates (especially considering the possible factor 2 error on the spectroscopic distances) or to proper motion selection effects.

The velocity of one subdwarf is so large as to suggest that this star is not gravitationally bound to the galaxy. The star LSR0400+5417, classified as an sdK7 has an estimated velocity relative to the local standard of rest $> 1300\text{km s}^{-1}$ (it cannot be seen in Fig 17, as it falls outside the limits of the plots). This star could be an actual extra-galactic object, but it is more likely that the large apparent velocity can be explained by an overestimated distance. We suggest that this star may actually be a misclassified extreme subdwarf, which we indicate by assigning the label (e)sdK7. In Table 4, we show in parenthesis the estimated distances and velocity components assuming the star is an esdK. The distance is reduced by more than a factor of two, and the star falls back into a gravitationally bound galactic

orbit. This illustrates well how errors in the spectral classification can dramatically affect the estimated distance and kinematics of M subdwarfs. A few other stars fall just beyond the limit of gravitationally bound orbits, but again this most likely reflects overestimated distances. Indeed it is possible that all the stars that lie beyond the 2σ limit of very metal-poor (halo) stars may have overestimated distances. As it turns out, most of these are currently classified as sdK/sdM (see Fig.17); if it turns out that these are also misclassified esdK/esdM stars, then they may in reality have velocities within the 2σ limit of halo stars.

At this point, we see no apparent difference between the velocity space distribution of the sdM and esdM stars, but any specific difference in their velocity distribution might be blurred by the large errors in the UVW components. In any case our sample is relatively small, and a more extensive study of the velocity distribution of a larger sample of low-mass subdwarfs and extreme subdwarfs would be most instructive.

5. Notes on Individual Objects of Interest

5.1. LSR0200+5530: a non-metal poor M dwarf with very large space motion

With a magnitude $R=19.7$, LSR0200+5530 is the faintest star in our sample. While our MDM spectrum for that star is particularly noisy, it strongly suggests a spectral type M5.5 V; the TiO bands are clearly too strong for the star to be a subdwarf. This then places the star at a distance $d=90\text{pc}$, with a surprisingly large space motion for a non metal-poor star ($U=-120\text{ km s}^{-1}$, $V=-200\text{ km s}^{-1}$). Thus, LSR0200+5530 appears to be a solar metallicity star, or perhaps a marginally metal poor star, on a halo-like orbit. Since it is unlikely that a non metal-poor star would originate in the halo itself, this star appears to be a clear example of a star born in the disk that later migrated to the halo. A close gravitational interaction with a binary in a dense star cluster, or evaporation from a massive cluster may have sent this one flying away.

5.2. LSR0400+5417: an extra-galactic star?

It is unclear whether LSR0400+5417 is a subdwarf (sdK) or an extreme subdwarf (esdK) star. While its spectrum is consistent with an sdK7 subtype, the inferred spectroscopic distance is very large ($d=375\text{pc}$) and suggests an enormous velocity relative to the l.s.r. ($\approx 1300\text{ km s}^{-1}$). If this is real, then this metal poor star is an extragalactic object that just happens to be moving through the Galaxy at this time. On the other hand LSR0400+5417 may actually be an intrinsically fainter esdK7 star at a much closer distance. Based on the

extreme subdwarf distance calibration, we estimate that as an esdK7, this star would be at $d=150\text{pc}$. This reduces the space motion to $\approx 550\text{km s}^{-1}$, which is still extremely large, but is at least consistent with the star being on an very eccentric, bound halo orbit.

5.3. LSR0419+4233: an ultra-cool M8.5V dwarf on a halo-like orbit

With a spectral type M8.5 Ve, this low-mass star is at a spectroscopic distance of only about 10pc. This star, however, has a very large proper motion ($\mu = 1.535'' \text{ yr}^{-1}$) which at a distance of 10pc translates into a velocity $> 90\text{km s}^{-1}$ relative to the local standard of rest). This space motion is unusually large for a non-metal poor disk star, and one has to wonder if the star might not actually be much closer, which would reduce its estimated velocity. At a distance of 10pc or larger, its velocity suggest that it might be a low-mass, local representative of the thick disk. This is clearly a high priority target for follow-up parallax measurements.

5.4. LSR0539+4038: a new nearby M8.0Ve dwarf.

This ultra-cool M8.0 Ve dwarf is estimated to be at a distance of only 10pc. Its large proper motion ($\mu = 1.057'' \text{ yr}^{-1}$) is clearly a result of its proximity. Again, this is an excellent candidate for inclusion in the census of very nearby stars.

5.5. LSR0549+2329: a white dwarf with halo-like kinematics?

This cool DC8 white dwarf appears to have a very large space motion typical of a star with halo kinematics: at least 260 km/sec and possibly larger, as the radial velocity is not measurable. This holds true even if we assume that its distance has been overestimated by up to a factor of 2. While this star might be a member of the hypothetical population of very old halo white dwarfs suggested by Oppenheimer *et al.* (2001), the fact that we are finding non-metal poor M dwarfs with halo kinematics (e.g. LSR0200+5530 above) suggest instead that this white dwarf was possibly born in the disk and eventually migrated to the halo.

5.6. LSR0556+1144: a bright, previously unreported, nearby dwarf

This relatively bright $R=14.2$ star is the second brightest of our sample. With a spectral type M5.5 V, it is also relatively cool and intrinsically faint, and has a spectroscopic distance of only 10pc. This is a good candidate for inclusion in the census of very nearby stars. The fact that this star is in a relatively crowded, low-galactic latitude field explains why it could have been missed in previous nearby star searches.

5.7. LSR1722+1004: a non-metal poor M dwarf ejected from the disk?

This is another M dwarf with disk-like abundances and halo-like kinematics. Its spectrum is clearly that of a metal-rich M4.0 V, but its spectroscopic distance of $d=70$ pc implies a very large space motion (≈ 250 km s⁻¹). The UVW velocity components suggest that this star is on a highly eccentric galactic orbit that brings it into the halo. Again, this could be a star initially born in the disk that later got ejected out to the halo.

5.8. LSR1802+0028: an extreme subdwarf on a very eccentric, retrograde halo orbit

This extreme subdwarf is very distant (spectroscopic distance $d=180$ pc), and it has an extremely large velocity relative to the local standard of rest, with an estimated $V=-640$ km s⁻¹. Even if its distance has been overestimated by a factor two (which would imply that this star fall on a sequence below that of even the extreme subdwarfs), it would still have $V < -500$ km s⁻¹ because of its extremely large radial velocity. There is little doubt that this exceptional object is a true halo star. Its spectrum actually shows very little trace of molecular TiO absorption. This most likely is an extremely metal poor star on a very eccentric, retrograde halo orbit.

5.9. LSR1833+2219: a companion to GJ718

This star is a companion to the nearby star GJ718A, also known as the flare star V774 Her. In a previous paper (Lepine, Shara, & Rich 2002a), we named this star GJ718B, and reported a spectral type M4.5 V. This spectral type was based on the G97 indices alone. The use of our expanded system yields a spectral type M5.0 V instead. The spectroscopic distance of 26pc is very close to the actual distance of 23.4pc measured by HIPPARCOS for

GJ718A (ESA 1997). This supports the idea that our spectroscopic distances are reasonably accurate, at least for the M dwarfs.

5.10. LSR1835+3259: an M9.0V star only 6 parsecs from the Sun

With a spectral type M9.0 V, LSR1835+3259 is the coolest star in our sample. Its optical and infrared magnitudes all are consistent with the star being at about 6pc from us. We note that only two other M9.0 dwarfs are known to be within 7pc of the sun: DENIS 1048-39 at a distance of about 4pc, and LP944-20 at a distance of about 5pc (Delfosse *et al.* 2001). This star is a prime candidate for follow-up astrometric parallax measurement.

5.11. LSR1914+2825AB: a pair of high velocity subdwarfs

This pair of early type subdwarf (sdM) stars is very peculiar because of their large spectroscopic distance. Assuming a distance of 200pc, the pair has a huge space motion of $\approx 500\text{km s}^{-1}$ relative to the local standard of rest, placing it on a halo orbit. The angular separation between the components of $\approx 12''$ implies a current orbital separation $> 2400\text{AU}$.

The 40% difference in the estimated distance of the two stars illustrates the relatively large errors that plague the distance estimates of sdM stars. Because the two stars most probably have the same metallicity, one might expect that errors related to the metallicity class assignment would be systematic, and that the relative estimated distances of the two stars should be relatively small. However, because the slope of the spectral-type/absolute magnitude calibration changes with metallicity (see Figs.13-14), errors on the relative distances may still occur because of the crude assignment in a monolithic metallicity class.

On the other hand, it is also possible that LSR1914+2825B is an unresolved binary. In this case, its distance might be underestimated by up to 40%, which would nicely explain the observed mismatch in the relative distances.

5.12. LSR1928-0200AB: a pair of M dwarfs in the halo?

This is a pair of M dwarfs with a large orbital separation. The earlier M3.5 V component LSR1928-0200A has a spectroscopic distance of 85pc, and the later M5.5 V component LSR1928-0200B has a spectroscopic distance of 65pc. Their $10''$ angular separation translates into a current orbital separation $\gtrsim 650\text{ AU}$. While the 30% relative distance is not inconsis-

tent with our estimated errors, it is possible that LSR1928-0200B might be an unresolved binary, with its distance somewhat underestimated. In any case, the relatively large distance of the pair translates into an extremely large space motion ($\approx 280\text{-}360 \text{ km s}^{-1}$ to the local standard of rest) that is atypical of non metal-poor stars.

The existence of such a system is quite puzzling. How can a non metal-poor, or slightly metal poor binary have halo-like kinematics? A very complex multi-body dynamical event in a cluster cannot be ruled out, but would be unlikely. A more reasonable explanation might be the evaporation of the system from a very massive cluster, in the scenario described in Kroupa (2002). Another possibility is that this system has been accreted by the Galaxy, possibly through a merger event with a slightly metal poor galaxy.

5.13. LSR1945+4650AB: a pair of cool white dwarfs

This is a pair of cool white dwarfs (DA9+DC10) for which we are having some problem in estimating their distance. The photometric distance derived for LSR1945+4650A (30pc) is half the photometric distance of its companion (60pc). The two stars are a clear common proper motion pair, and the chances are extremely small that they are not physically related. With a $\approx 9''$ angular separation, the two stars are probably several hundred AU apart. The apparent discrepancy in the estimated photometric distances rather suggests that the method is prone to relatively large errors. The photometric distance is based on the B-R color term (Equation 26). Both B and R are derived from photographic plates, and accurate to only about 0.5 magnitudes. Therefore, B-R is accurate to about 0.7 magnitudes, which can lead to a 40% error in the distance estimate of a single object, which means that there typically is a factor 2 error in the relative estimated distance between two stars. It is also possible that LSR1945+4650A is itself a pair of spatially unresolved white dwarfs, in which case our distance of 30pc could be significantly underestimated.

5.14. LSR2036+5059: the coolest known subdwarf

We find for this star a spectral type sdM7.5, which is unusually late for a subdwarf. As far as we know, LSR2036+5059 is the coolest M subdwarf reported to date. The coolest subdwarf reported in the literature so far was LHS377, with a spectral type sdM7.0 (Gizis 1997). The spectrum of LSR2036+5059 is distinctly odd-looking with its very deep CaH band and relatively weak TiO features (see Figure 7). With a transverse velocity of $\sim 90 \text{ km s}^{-1}$, it is a possible member of the old-disk population. This star could have a mass extremely

close to the hydrogen burning limit for metal poor stars. At a spectroscopic distance of only 18pc, this subdwarf is also a very likely member of the Solar Neighborhood.

5.15. LSR2122+3656: a very cool, extreme subdwarf

This star, with spectral type esdM5.0, is the coolest extreme subdwarf in our sample. The coolest extreme subdwarf known to date is the esdM7 star APMPM J0559-2903 (Schweitzer *et al.* 1999). LSR2122+3656 is also the closest esdM in our sample, at a spectroscopic distance of 45pc. This emphasizes the extreme rarity of the esdM stars in the Solar Neighborhood, and shows the effectiveness of high proper motion surveys in recovering them.

5.16. LSR2124+4003: an M6.5V star only 7 parsecs from the Sun

This cool red dwarf (M6.5 V) was among the brightest stars in our sample (R=14.9). With a spectroscopic distance of about 7pc, it may prove to be among the 100 nearest systems. Along with LSR1835+3259, this is a top candidate for follow-up, astrometric parallax measurements.

6. Conclusions

We have obtained spectra for 104 new stars with large proper motions ($\mu > 0.5'' \text{ yr}^{-1}$) found at low galactic latitudes (Lepine, Shara, & Rich 2002b). We find that 54 of the targets are M dwarfs (M), 25 are subdwarfs (sdK, sdM), 14 are extreme subdwarfs (esdK, esdM), and 11 are late-type DA and DC white dwarfs.

We have expanded and refined the G97 classification method for M dwarfs and subdwarfs by defining a larger set of spectral indices whose calibration with spectral type can be used for spectral classification. The new scheme can be applied to perform spectral classification of all M dwarfs (early and late-type), subdwarfs, and extreme subdwarfs, from a spectrum covering the 6000Å-9000Å wavelength range. Among the M dwarfs classified in this paper, 8 have a spectral subtype M7 and later, including one new M9.0V star. We also find one subdwarf with a very late spectral type of sdM7.5, the coolest subdwarf ever reported.

We have provided a crude classification of the 11 white dwarf stars, from blackbody fits of the spectral energy distribution in the 6000Å-9000Å range. All the white dwarfs are relatively cool DA and DC, with the warmest at DC8 (6500K) and the coolest at DC11

(4750K). Many of the DC spectra are relatively noisy, and the DC spectral class was assigned only by default, for lack of clear identification of $H\alpha$ absorption. We thus suspect some of our DCs might be actual cool DAs.

We have derived a spectral-type / absolute magnitude calibration using sets of M, sdM, and esdM stars with published astrometric parallaxes. We have found the counterparts of those stars in the Guide Star Catalog-II (GSC2.2.1) and in the 2MASS Second Incremental Release, to obtain their observed B, R, and K_s magnitudes. The spectral-type / absolute magnitude relationships for M dwarfs was modeled with a third order polynomial, while we fit a linear relationship for the sdM and esdM stars. Using the empirically determined spectral-type / absolute magnitude relationships, we have determined spectroscopic distances for all the observed red dwarfs and subdwarfs in our sample.

We have obtained crude radial velocity measurements for most of our stars using centroid measurements of Na I, K I, Ca I, and Ca II atomic absorption lines. Combining these radial velocities with the estimated distances and proper motions, we estimate the UVW velocity components (measured relative to the local standard of rest) of all the stars. The distribution of M dwarf stars in UVW space is consistent with most of the stars being components of the disk. However, some have velocities that are more consistent with halo orbits, which is quite surprising for non-metal poor stars. We suggest that these stars originate in the disk but got ejected into halo orbits through some yet undefined mechanism. Possible scenarios include 3-body gravitational interactions or massive cluster evaporation.

While we find the UVW space distribution of white dwarfs to be similar to that of the M dwarfs, the velocity space distribution of subdwarfs and extreme subdwarfs is markedly different, and is largely consistent with the distribution of known, very metal-poor, candidate halo stars. We find that a significant number of sdM and esdM stars fall outside the 2σ limit of halo stars in UVW space. These stars are apparently on very eccentric halo orbits, some of which appear to be at the limit of being gravitationally bound to the Galaxy.

Finally, we report the discovery of a number of new, very nearby stars, including two stars that are most likely to be well within 10pc of the Sun, and 29 more (25 M dwarfs, 3 white dwarfs, and 1 subdwarf) that are likely to be within 25pc of the Sun. The two new very nearby stars are LSR1835+3259, an M9.0 dwarf at about 6pc, and LSR2124+4003, and M6.5 dwarf at about 7pc from the Sun.

Follow-up spectroscopy of newly discovered faint stars with large proper motions proves yet again to be very productive in recovering intrinsically faint stars in the Solar neighborhood, and faint stars with extreme transverse velocity components (possibly halo stars). Our spectroscopic follow-up survey of new high proper motion stars is still in progress, and

is being expanded as new northern stars with large proper motions are being discovered. Future results will be presented in upcoming papers in this series.

This research program is being supported by NSF grant AST-0087313 at the American Museum of Natural History, as part of the NStars program.

This work has been made possible through the use of the Guide Star Catalogue-II. The Guide Star Catalogue-II is a joint project of the Space Telescope Science Institute and the Osservatorio Astronomico di Torino. Space Telescope Science Institute is operated by the Association of Universities for Research in Astronomy, for the National Aeronautics and Space Administration under contract NAS5-26555. The participation of the Osservatorio Astronomico di Torino is supported by the Italian Council for Research in Astronomy. Additional support is provided by European Southern Observatory, Space Telescope European Coordinating Facility, the International GEMINI project and the European Space Agency Astrophysics Division.

This publication makes use of data products from the Two Micron All Sky Survey, which is a joint project of the University of Massachusetts and the Infrared Processing and Analysis Center, funded by the National Aeronautics and Space Administration and the National Science Foundation.

The data mining required for this work has been made possible with the use of the SIMBAD astronomical database and VIZIER astronomical catalogs service, both maintained and operated by the Centre de Données Astronomiques de Strasbourg (<http://cdsweb.u-strasbg.fr/>).

We thank the anonymous referee for a very thorough review, which lead to a significant improvement of the manuscript.

REFERENCES

- Chiba, M., & Beers, T. 2000, *AJ*, 119, 2843
- Cruz, K. L., & Reid, I. N. 2002, *AJ*, 123, 2828
- Dahn, C. C., Harris, H. C., Vrba, F. J., Guetter, H. H., Canzian, B., Henden, A. A., Levine, S. E., Luginbuhl, C. B., Monet, A. K. B., Monet, D. G., Pier, J. R., Stone, R. C., Walker, R. L., Burgasser, Adam J., Gizis, J. E., Kirkpatrick, J. D., Liebert, J., & Reid, I. N. 2002, *AJ*, 124, 1170

- Dauphole, B., & Colin, J. 1995, *A&A*, 300, 117
- Dehnen, W., & Binney, J. J. 1998, *MNRAS*, 298, 387
- Delfosse, X., Tinney, C. G., Forveille, T., Epchtein, N., Borsenberger, J., Fouqué, P., Kimeswenger, S., & Tiphène, D. 1999, *A&AS*, 135, 41
- Delfosse, X., Forveille, T., Martín, E. L., Guibert, J., Borsenberger, J., Crifo, F., Alard, C., Epchtein, N., Fouqué, P., Simon, G., & Tajahmady, F. 2001, *A&A*, 366, L13
- ESA, 1997, *The Hipparcos and Tycho Catalogues*, ESA SP-1200 (*CDS-ViZier catalog number I/239*)
- Gizis, J. E. 1997, *AJ*, 113, 806 (G97)
- Gizis, J. E., & Reid, I. N. 1997, *PASP*, 109, 849
- Gizis, J. E., Monet, D. G., Reid, I. N., Kirkpatrick, J. D., Liebert, J., & Williams, R. J. 2000, *AJ*, 120, 1085
- Henry, T. J., Ianna, P. A., Kirkpatrick, J. D., & Jahreiss, H. 1997, *AJ*, 114, 388
- Henry, T. J., Walkowicz, L. M., Barto, T. C., & Golimowski, D. A. 2002, *AJ*, 123, 2002
- Hawley, S. L., *et al.* 2002, *AJ*, 123, 3409
- Hurley, J. R., Shara, & M. M. 2002, *ApJ*, 570, 184
- Jahreiss, H., Scholz, R., Meusinger, H., & Lehmann, I. 2001, *A&A*, 370, 967
- Kirkpatrick, J. D., Henry, T. J., & McCarthy, D. W. 1991, *ApJS*, 77, 417
- Kirkpatrick, J. D., Henry, T. J., Simons, D. A. 1995, *AJ*, 109, 797
- Kirkpatrick, J. D., Reid, I. N., Liebert, J., Cutri, R. M., Nelson, B., Beichman, C. A., Dahn, C. C., Monet, D. G., Gizis, J. E., & Skrutskie, M. F. 1999, *ApJ*, 519, 802
- Kroupa, P. 2002, *MNRAS*, 330, 707
- Lépine, S., Shara, M. M., & Rich, R. M. 2002a, *AJ*, 123, 3434
- Lépine, S., Shara, M. M., & Rich, R. M. 2002b, *AJ*, 124, 1190
- Luyten W. J. 1925, *ApJ*, 62, 8

- Luyten W. J. 1979, LHS Catalogue: a catalogue of stars with proper motions exceeding 0.5" annually, University of Minnesota, Minneapolis (*CDS-ViZier catalog number I/87B*)
- Luyten W. J. 1980, New Luyten Catalogue of stars with proper motions larger than two tenths of an arcsecond (NLTT), University of Minnesota, Minneapolis (*CDS-ViZier catalog number I/98A*)
- Martín, E. L., Delfosse, X., Basri, G., Goldman, B., Forveille, T., Zapatero Osorio, M. R. 1999, *AJ*, 118, 2466
- Massey, P., Strobel, K., Barnes, J. V., Anderson, E. 1988, *ApJ*, 328, 315
- Massey, P., & Gronwall, C. 1990, *ApJ*, 358, 344
- Oppenheimer, B. R., Hambly, N. C., Digby, A. P., Hodgkin, S. T., & Saumon, D. 2001, *Science*, Volume 292, Issue 5517, pp. 698-702
- Phan-Bao, N., Guibert, J., Crifo, F., Delfosse, X., Forveille, T., Borsenberger, J., Epchtein, N., Fouqué, P., & Simon, G. 2001, *A&A*, 380, 590
- Raboud, D., Grenon, M., Martinet, L., Fux, R., & Udry, S. 1998 *A&A*, 335, L61
- Reid, I. N., Hawley, S. L., & Gizis, J. E. 1995, *AJ*, 110, 1838
- Reid, I. N., Liebert, J., & Schmidt, G. 2001, *ApJ*, 550, L61
- Reid, I. N., Kilkeny, D., & Cruz, K. L. 2002, *AJ*, 123, 2822
- Reylé, C., Robin, A. C., Scholz, R.-D., & Irwin, M. 2002, *A&A*, 390, 491
- Salim, S., & Gould, A. 2002, *ApJ*, 575, L83
- Scholz, R.-D., Irwin, M., Ibata, R., Jahreiss, H., & Malkov, O. Yu. 2000, *A&A*, 353, 958
- Scholz, R.-D., Ibata, R., Irwin, M., Salvato, M., & Schweitzer, A. 2002a, *MNRAS*, 329, 109
- Scholz, R.-D., Szokoly, G. P., Andersen, M., Ibata, R., & Irwin, M. J. 2002b, *ApJ*, 565, 539
- Schweitzer, A., Scholz, R.-D., Stauffer, J., Irwin, M., & McCaughrean, M. J. 1999, *A&A*, 350, L62
- Wesemael, F., Greenstein, J. L., Liebert, James, Lamontagne, R., Fontaine, G., Bergeron, P., & Glaspey, J. W. 1993, *PASP*, 105, 761

Table 1. Newly classified high proper motion stars

Star	μ (″ yr ⁻¹)	pma (deg)	B	R	K _s	Date of spec.	Obs. ¹	Sp. type ²	HRV(km s ⁻¹) ³
LSR0011+5908	1.483	218.3	...	14.5	...	2001-07-24	L	M5.5 V	+90±40
LSR0014+6546	0.962	67.2	18.0	15.7	...	2001-07-24	L	sdM4.5	-150±40
LSR0020+5526	0.541	55.7	17.2	14.9	...	2001-02-03	M	esdM2.5	-100±50
LSR0124+6819	0.559	131.4	18.9	16.4	...	2001-12-08	L	M7.0 V	-10±30
LSR0134+6459	0.924	75.5	17.9	15.2	...	2001-12-08	L	M5.5 V	+0±30
LSR0155+3758	0.538	153.9	17.0	14.8	9.6	2001-07-24	L	M5.0 V	-60±40
LSR0157+5308	0.641	94.7	17.1	14.9	11.3	2001-02-02	M	sdM3.5	-30±30
LSR0200+5530	0.507	112.0	...	19.7	...	2001-02-05	M	M5.5 V	-70±50
LSR0212+7012	0.744	76.2	18.4	15.9	...	2001-12-08	L	M5.0 V	+10±30
LSR0258+5354	0.545	127.7	17.2	14.9	12.6	2001-02-02	M	sdK7	+130±30
LSR0310+6634	0.808	121.6	...	17.5	...	2001-07-25	L	DC10	...
LSR0316+3132	0.759	139.2	17.7	15.4	10.6	2001-12-08	L	M5.0 V	+100±30
LSR0340+5124	0.932	155.9	17.6	15.4	...	2001-02-01	M	M5.5 V	-30±30
LSR0342+5527	0.500	145.8	17.0	14.8	...	2001-02-04	M	sdM0.0	+90±30
LSR0354+3333	0.848	150.2	...	16.4	10.9	2001-02-02	M	M6.0 V	+70±30
LSR0358+8111	0.547	143.8	19.0	16.9	13.6	2001-12-08	L	sdM1.5	-30±30
LSR0400+5417	0.754	136.7	18.0	16.0	...	2001-02-04	M	(e)sdK7	-150±30
LSR0401+5131	0.886	156.0	17.9	16.7	...	2001-02-04	M	DC8	...
LSR0419+4233	1.535	159.4	...	17.4	...	2001-02-02	M	M8.5 Ve	+30±30
LSR0455+0244	0.768	123.2	18.5	16.4	...	2001-12-08	L	M5.5 V	+60±30
LSR0455+5252	0.804	187.8	...	18.3	...	2001-02-02	M	M8.0 Ve	-30±30
LSR0505+3043	1.097	148.5	18.5	16.0	...	2001-02-01	M	esdM3.5	+210±30
LSR0505+6633	0.577	155.1	...	17.0	...	2001-07-26	L	sdM4.5	-90±40
LSR0515+5911	1.015	173.3	...	16.8	...	2001-07-26	L	M7.0 V	-60±40
LSR0519+4213	1.181	139.5	...	16.1	12.9	2001-02-04	M	esdM3.5	-280±30
LSR0521+3425	0.512	149.2	18.1	15.8	11.0	2001-02-04	M	M5.0 V	+60±30
LSR0522+3814	1.703	164.1	16.6	14.5	12.6	2001-02-01	M	esdM3.0	-110±30
LSR0524+3358	0.530	138.4	...	17.5	14.1	2001-02-04	M	sdM1.5	-190±50
LSR0527+3009	0.639	221.0	...	16.3	11.5	2001-02-05	M	M5.0 V	+0±30
LSR0533+3837	0.551	134.9	18.1	16.3	13.1	2001-02-05	M	sdM2.0	-170±30
LSR0539+4038	1.057	141.8	...	17.0	10.0	2001-02-01	M	M8.0 Ve	+10±30
LSR0541+3959	0.566	143.2	18.1	17.1	15.3	2001-02-05	M	DA8	+10±30
LSR0549+2329	1.379	131.4	...	17.4	...	2001-02-02	M	DC8	...
LSR0556+1144	0.611	121.8	16.5	14.2	...	2001-12-08	L	M5.5 V	+160±30
LSR0609+2319	1.104	130.7	18.7	16.5	12.4	2001-12-08	L	sdM5.0	-40±30
LSR0618+1614	0.646	165.7	16.9	14.7	11.9	2001-02-04	M	sdM2.0	+70±30
LSR0621+3652	0.865	176.9	16.6	14.5	11.9	2001-02-02	M	esdK7	+230±30
LSR0627+0616	1.019	178.5	17.6	15.4	...	2001-02-01	M	esdM1.5	-130±30
LSR0628+0529	0.551	140.4	...	17.1	...	2001-02-05	M	M7.0 V	+110±30
LSR0646+3212	0.567	142.4	...	17.5	13.1	2001-02-05	M	M5.5 V	+170±80
LSR0702+2154	0.653	144.7	16.9	14.9	10.3	2001-02-02	M	M5.5 V	+20±30
LSR0705+0506	0.510	158.4	18.8	16.0	...	2001-02-04	M	sdM3.5	+100±50
LSR0721+3714	0.587	234.7	18.9	16.2	10.8	2001-02-02	M	M5.5 Ve	+60±30
LSR0731+0729	0.512	190.3	17.3	15.2	...	2001-02-02	M	M5.0 V	+150±50
LSR0803+1547	0.516	154.3	18.4	16.1	13.4	2001-02-02	M	sdM0.0	-140±30
LSR1722+1004	0.724	192.1	17.5	15.1	...	2001-07-24	L	M4.0 V	-10±40
LSR1755+1648	0.995	116.9	16.4	14.2	...	2001-07-24	L	sdM3.5	-30±40
LSR1757+0015	0.518	184.8	19.4	17.0	...	2001-07-24	L	sdM4.5	+10±40
LSR1758+1417	1.014	235.4	16.9	15.8	14.6	2001-07-24	L	DA10	...

Table 1—Continued

Star	μ (″ yr ⁻¹)	pma (deg)	B	R	K _s	Date of spec.	Obs. ¹	Sp. type ²	HRV(km s ⁻¹) ³
LSR1802+0028	0.543	211.3	...	17.6	...	2001-07-26	L	esdM1.5	-480±40
LSR1806+1141	0.541	186.0	16.5	14.4	...	2001-07-26	L	M4.0 V	+10±40
LSR1808+1134	0.606	228.7	16.8	14.4	...	2001-07-26	L	M5.0 V	+10±40
LSR1809-0219	0.506	176.0	16.4	13.9	9.3	2001-07-25	L	M4.5 V	+40±40
LSR1809-0247	1.005	214.9	17.4	15.2	10.7	2001-07-25	L	M5.0 V	-80±40
LSR1817+1328	1.207	201.5	16.7	15.5	...	2001-07-25	L	DA10	-40±40
LSR1820-0031	0.555	199.3	17.8	15.7	...	2001-07-26	L	sdM2.0	-10±40
LSR1833+2219	0.502	200.0	17.6	14.9	...	2001-07-24	L	M5.0 V	+40±30
LSR1835+3259	0.747	185.8	...	16.6	9.2	2002-05-25	M	M9.0 Ve	-10±40
LSR1836+1040	0.921	206.0	18.2	15.9	...	2001-07-25	L	esdM0.5	-150±40
LSR1841+2421	0.752	189.0	19.0	16.5	...	2001-02-03	M	M6.0 V	+30±30
LSR1843+0507	0.577	253.2	19.2	17.1	...	2001-07-26	L	M5.5 V	-50±40
LSR1844+0947	0.501	224.3	17.6	15.8	...	2001-07-26	L	(sd)M2.0V	-90±40
LSR1851+2641	0.704	26.3	18.9	16.1	...	2001-02-03	M	M6.0 Ve	+10±30
LSR1859+0156	0.674	142.2	16.9	14.7	...	2001-07-26	L	M4.5 V	-90±40
LSR1914+2825A	0.529	212.6	17.5	15.0	...	2001-07-26	L	sdM0.0	-80±40
LSR1914+2825B	0.531	214.3	18.7	15.6	...	2001-07-26	L	sdM1.5	-120±40
LSR1918+1728	0.626	192.2	...	17.2	...	2001-07-25	L	esdM3.0	-160±40
LSR1919+1438	0.507	96.6	...	14.9	...	2001-07-26	L	M5.0 V	-20±40
LSR1922+4605	0.555	206.3	17.8	15.1	12.9	2002-05-25	M	sdM0.0	-20±40
LSR1927+6802	0.515	227.2	...	17.2	...	2002-05-25	M	M6.5 V	-20±40
LSR1928-0200A	0.858	194.7	...	15.2	11.3	2001-07-25	L	M3.5 V	-100±40
LSR1928-0200B	0.858	194.7	...	18.2	13.1	2001-07-25	L	M5.5 V	-80±40
LSR1933-0138	0.895	132.6	15.6	13.5	10.1	2001-07-26	L	M3.0 V	-170±40
LSR1943+0941	0.543	213.6	18.7	16.2	...	2002-05-25	M	M5.5 V	+0±40
LSR1945+4650A	0.612	228.0	17.9	16.8	15.5	2002-05-25	M	DA9	...
LSR1945+4650B	0.609	228.7	19.3	17.0	15.2	2002-05-25	M	DC10	...
LSR1946+0937	0.566	173.7	17.5	16.8	...	2001-07-26	L	DA9	-140±40
LSR1946+0942	0.555	173.8	16.8	14.6	...	2001-07-26	L	M3.5 V	-130±40
LSR1956+4428	0.891	214.3	17.3	15.0	...	2000-08-01	L	esdM0.5	-140±30
LSR2000+0404	0.503	125.1	18.0	15.7	...	2001-07-26	L	M5.5 V	+20±40
LSR2000+3057	1.339	16.7	...	15.6	9.7	2001-07-24	L	M6.0 Ve	-10±40
LSR2005+0835	0.583	197.9	16.5	14.6	...	2001-07-26	L	sdK5	-20±40
LSR2009+5659	0.824	31.5	16.3	14.2	11.2	2001-07-25	L	sdM2.0	-120±40
LSR2010+3938	0.512	180.4	17.4	13.3	11.8	2000-08-01	L	(sd)M1.5V	-210±30
LSR2013+0417	0.749	195.5	16.2	14.4	...	2001-07-25	L	sdK7	-190±40
LSR2017+0623	0.674	187.3	18.2	16.0	...	2001-07-25	L	M5.0 V	+20±40
LSR2036+5059	1.054	100.8	...	16.8	...	2001-12-09	L	sdM7.5	-140±30
LSR2044+1339	0.518	31.2	15.4	15.4	10.3	2001-07-26	L	M5.0 Ve	-20±40
LSR2050+7740	0.543	27.3	19.3	18.0	...	2002-05-20	K	DC11	...
LSR2059+5517	0.500	33.1	18.2	16.8	...	2002-05-25	M	DC11	...
LSR2107+3600	0.736	231.4	18.4	15.9	11.7	2001-07-25	L	M4.5 V	-130±40
LSR2115+3804	0.506	25.2	17.3	15.0	12.3	2001-07-26	L	esdK7	-140±40
LSR2117+7345	0.746	41.1	18.6	16.4	...	2001-07-24	L	M6.0 V	+70±40
LSR2122+3656	0.816	65.0	18.7	16.2	...	2001-07-24	L	esdM5.0	-100±40
LSR2124+4003	0.697	50.9	17.3	14.9	...	2000-08-02	L	M6.5 V	-60±30
LSR2132+4754	0.569	37.8	16.8	14.5	10.7	2001-07-26	L	M4.0 V	-60±40
LSR2146+5147	0.584	49.7	18.5	16.0	...	2001-07-26	L	sdM1.0	-210±40
LSR2158+6117	0.819	82.3	17.9	15.7	...	2001-07-24	L	M6.0 V	-70±40

Table 1—Continued

Star	μ (″ yr ⁻¹)	pma (deg)	B	R	K _s	Date of spec.	Obs. ¹	Sp. type ²	HRV(km s ⁻¹) ³
LSR2205+5353	0.528	236.4	17.3	15.1	...	2001-07-25	L	sdM1.0	-200±40
LSR2205+5807	0.538	108.9	17.9	17.6	...	2001-07-26	L	esdM1.0	-130±40
LSR2251+4706	0.631	71.5	...	17.9	12.6	2001-07-25	L	M6.5 V	-100±40
LSR2311+5032	0.669	81.0	16.9	14.6	9.9	2001-02-03	M	M4.5 V	-30±30
LSR2311+5103	0.531	253.5	...	18.1	12.3	2001-07-25	L	M7.5 V	-10±40
LSR2321+4704	0.712	70.5	18.5	16.2	13.2	2001-12-08	L	esdM2.0	-220±30

¹Observatory used: Lick 3m Shane (L), MDM 2.4m Hiltner (M), KPNO 4m Mayall (K)

²Spectral class and subtype based on spectroscopy. Parenthesis indicates possible change in spectral class required for consistency with the star’s kinematics.

³Estimated heliocentric radial velocity.

Table 2. Spectral Type Indices for M dwarfs and subdwarfs

Index Name	Numerator	Denominator	Other Name	Ref.
CaH1	6380-6390	Avg. of 6410-6420 and 6345-6355	...	Reid <i>et al.</i> 1995
CaH2	6814-6846	7042-7046	...	Reid <i>et al.</i> 1995
CaH3	6960-6990	7042-7046	...	Reid <i>et al.</i> 1995
TiO5	7126-7135	7042-7046	...	Reid <i>et al.</i> 1995
VO1	7430-7470	7550-7570	VO 7434	Hawley <i>et al.</i> 2002
TiO6	7550-7570	7745-7765	...	this paper
VO2	7920-7960	8130-8150	...	this paper
TiO7	8440-8470	8400-8420	TiO 8440	Hawley <i>et al.</i> 2002
Color-M	8105-8155	6510-6560	...	this paper

Table 3. Measured Spectral Indices of observed M dwarfs, subdwarfs, and extreme subdwarfs

Star	CaH1	CaH2	CaH3	TiO5	VO1	TiO6	VO2	TiO7	Color-M	Sp. Type
LSR0011+5908	0.774	0.266	0.556	0.214	0.843	0.548	0.641	0.739	3.632	M5.5V
LSR0014+6546	0.574	0.369	0.575	0.628	0.926	0.984	0.954	0.994	1.479	sdM4.5
LSR0020+5526	0.566	0.471	0.654	0.986	0.964	1.025	0.896	1.070	1.568	esdM2.5
LSR0124+6819	0.928	0.294	0.625	0.223	0.776	0.483	0.489	0.595	5.519	M7.0V
LSR0134+6459	0.848	0.340	0.664	0.270	0.874	0.580	0.631	0.742	3.600	M5.5V
LSR0155+3758	0.823	0.378	0.685	0.326	0.861	0.581	0.682	0.802	2.833	M5.0V
LSR0157+5308	0.681	0.426	0.630	0.505	0.975	0.827	0.915	0.913	1.200	sdM3.5
LSR0200+5530	0.498	0.254	0.538	0.238	0.743	0.495	0.842	0.811	4.247	M5.5V
LSR0212+7012	0.673	0.224	0.570	0.201	0.818	0.663	0.730	0.795	3.721	M5.0V
LSR0258+5354	0.898	0.844	0.941	0.958	0.967	0.949	0.983	0.916	1.053	sdK7
LSR0316+3132	0.799	0.364	0.647	0.293	0.883	0.656	0.696	0.799	3.023	M5.0V
LSR0340+5124	0.831	0.349	0.629	0.326	0.900	0.609	0.683	0.603	2.918	M5.5V
LSR0342+5527	0.803	0.733	0.866	0.925	0.983	0.976	1.028	1.073	0.980	sdM0.0
LSR0354+3333	0.829	0.305	0.652	0.236	0.854	0.492	0.555	0.635	3.317	M6.0V
LSR0358+8111	0.660	0.571	0.795	0.802	0.991	0.989	1.009	1.013	1.355	sdM1.5
LSR0400+5417	0.879	0.776	0.868	0.884	0.969	0.944	1.112	1.715	0.947	(e)sdK7
LSR0419+4233	0.923	0.362	0.716	0.315	0.762	0.457	0.349	0.467	7.267	M8.5Ve
LSR0455+0244	0.672	0.252	0.539	0.284	0.860	0.572	0.648	0.776	3.636	M5.5V
LSR0455+5252	0.750	0.238	0.517	0.112	0.811	0.321	0.417	0.426	5.076	M8.0Ve
LSR0505+3043	0.616	0.397	0.626	0.797	0.961	0.901	0.887	0.799	1.316	esdM3.5
LSR0505+6633	0.500	0.340	0.584	0.591	1.017	1.071	0.955	1.006	1.426	sdM4.5
LSR0515+5911	0.808	0.257	0.563	0.209	0.814	0.453	0.471	0.612	6.112	M7.0V
LSR0519+4213	0.659	0.414	0.583	0.785	0.951	0.993	1.045	0.980	1.124	esdM3.5
LSR0521+3425	0.828	0.380	0.691	0.303	0.885	0.579	0.721	0.776	2.245	M5.0V
LSR0522+3814	0.566	0.462	0.642	0.970	0.965	1.027	0.900	1.064	1.588	esdM3.0
LSR0524+3358	0.945	0.589	0.787	0.810	0.924	0.916	0.967	1.050	1.247	sdM1.5
LSR0527+3009	0.778	0.295	0.591	0.266	0.928	0.633	0.690	0.801	2.669	M5.0V
LSR0533+3837	0.690	0.533	0.758	0.776	0.950	0.942	1.001	0.905	1.362	sdM2.0
LSR0539+4038	0.854	0.216	0.544	0.158	0.846	0.371	0.395	0.436	5.494	M8.0Ve
LSR0556+1144	0.772	0.324	0.649	0.252	0.850	0.546	0.600	0.712	3.864	M5.5V
LSR0609+2319	0.660	0.322	0.553	0.364	0.911	0.800	0.835	0.899	2.188	sdM5.0
LSR0618+1614	0.724	0.534	0.760	0.812	1.010	0.998	1.006	0.840	1.176	sdM2.0
LSR0621+3652	0.827	0.768	0.896	0.981	1.025	1.017	0.989	1.047	1.104	esdK7
LSR0627+0616	0.683	0.583	0.772	0.950	0.998	0.952	0.887	1.017	1.327	esdM1.5
LSR0628+0529	0.836	0.228	0.583	0.210	0.837	0.473	0.514	0.595	5.167	M7.0V
LSR0646+3212	0.596	0.312	0.555	0.171	0.838	0.708	0.661	1.135	5.019	M5.5V
LSR0702+2154	0.801	0.353	0.680	0.307	0.890	0.542	0.630	0.771	2.530	M5.5V
LSR0705+0506	0.688	0.399	0.648	0.536	0.974	0.832	0.914	0.863	1.255	sdM3.5
LSR0721+3714	0.803	0.295	0.593	0.254	0.856	0.530	0.628	0.716	3.533	M5.5Ve
LSR0731+0729	0.832	0.346	0.674	0.301	0.907	0.581	0.697	0.741	2.780	M5.0V
LSR0803+1548	0.781	0.723	0.818	0.927	1.005	0.913	1.080	0.882	1.330	sdM0.0
LSR1722+1004	0.789	0.403	0.679	0.397	0.932	0.710	0.814	0.897	2.029	M4.0V
LSR1755+1648	0.707	0.419	0.664	0.486	0.943	0.814	0.886	0.953	1.691	sdM3.5
LSR1757+0015	0.666	0.356	0.599	0.429	0.935	0.783	0.835	0.951	1.947	sdM4.5
LSR1802+0028	0.833	0.570	0.757	0.998	0.981	1.040	0.967	1.082	1.295	esdM1.5
LSR1806+1141	0.846	0.435	0.718	0.392	0.926	0.666	0.751	0.862	2.307	M4.0V
LSR1808+1134	0.907	0.409	0.720	0.330	0.894	0.586	0.658	0.780	2.943	M5.0V
LSR1809-0219	0.816	0.364	0.644	0.330	0.904	0.643	0.713	0.805	2.684	M4.5V
LSR1809-0247	0.765	0.313	0.594	0.272	0.918	0.624	0.722	0.827	2.639	M5.0V

Table 3—Continued

Star	CaH1	CaH2	CaH3	TiO5	VO1	TiO6	VO2	TiO7	Color-M	Sp. Type
LSR1820-0031	0.737	0.518	0.711	0.658	1.010	0.901	0.933	1.017	1.440	sdM2.0
LSR1833+2219B	0.827	0.362	0.662	0.304	0.885	0.595	0.688	0.792	2.711	M5.0V
LSR1835+3259	0.806	0.279	0.547	0.277	0.812	0.454	0.323	0.452	13.194	M9.0Ve
LSR1836+1040	0.754	0.678	0.812	0.990	0.984	1.042	0.981	1.050	1.176	esdM0.5
LSR1841+2421	0.741	0.245	0.565	0.230	0.862	0.519	0.653	0.611	4.387	M6.0V
LSR1843+0507	0.813	0.303	0.587	0.251	0.891	0.536	0.625	0.752	3.412	M5.5V
LSR1844+0947	0.802	0.515	0.749	0.547	0.969	0.830	0.873	0.965	1.600	(sd)M2.0V
LSR1851+2641	0.758	0.235	0.515	0.200	0.882	0.564	0.646	0.619	4.177	M6.0Ve
LSR1859+0156	0.816	0.375	0.664	0.318	0.912	0.603	0.697	0.841	2.651	M4.5V
LSR1914+2825A	0.821	0.691	0.844	0.821	0.953	0.939	0.954	1.015	1.260	sdM0.0
LSR1914+2825B	0.766	0.560	0.748	0.742	0.987	0.941	0.936	1.014	1.382	sdM1.5
LSR1918+1728	0.647	0.439	0.666	0.830	0.968	1.034	0.986	0.979	1.340	esdM3.0
LSR1919+1438	0.808	0.364	0.661	0.307	0.901	0.596	0.671	0.797	2.978	M5.0V
LSR1922+4605	0.795	0.729	0.835	0.854	0.983	1.011	0.970	0.994	1.259	sdM0.0
LSR1927+6802	0.746	0.326	0.688	0.225	0.852	0.510	0.546	0.662	4.693	M6.5V
LSR1928-0200A	0.851	0.474	0.735	0.460	0.940	0.719	0.844	0.939	1.773	M3.5V
LSR1928-0200B	0.840	0.295	0.602	0.235	0.887	0.539	0.630	0.768	3.340	M5.5V
LSR1933-0138	0.818	0.476	0.735	0.480	0.952	0.747	0.849	0.988	1.743	M3.0V
LSR1943+0941	0.908	0.336	0.652	0.269	0.867	0.570	0.598	0.733	3.673	M5.5V
LSR1946+0942	0.732	0.423	0.676	0.478	0.938	0.780	0.852	0.960	1.763	M3.5V
LSR1956+4428	0.000	0.679	0.820	1.011	0.979	1.034	0.960	1.035	1.303	esdM0.5
LSR2000+0404	0.850	0.308	0.610	0.243	0.875	0.511	0.604	0.751	3.589	M5.5V
LSR2000+3057	0.770	0.246	0.521	0.198	0.855	0.514	0.613	0.708	4.064	M6.0Ve
LSR2005+0835	0.959	0.954	0.978	1.025	0.991	0.969	0.981	1.019	1.054	sdK5
LSR2009+5659	0.678	0.519	0.718	0.758	0.967	0.981	0.974	1.017	1.304	sdM2.0
LSR2010+3938	0.000	0.552	0.785	0.667	0.971	0.917	0.882	1.002	1.562	(sd)M1.5V
LSR2013+0417	0.924	0.893	0.927	0.997	0.997	0.988	1.002	1.023	1.042	sdK7
LSR2017+0623	0.800	0.311	0.597	0.288	0.896	0.640	0.736	0.837	2.683	M5.0V
LSR2036+5059	0.572	0.173	0.366	0.263	0.867	0.816	0.841	0.894	2.788	sdM7.5
LSR2044+1339	0.811	0.349	0.629	0.314	0.886	0.593	0.695	0.810	2.868	M5.0Ve
LSR2107+3600	0.735	0.353	0.620	0.350	0.892	0.688	0.779	0.863	2.271	M4.5V
LSR2115+3804	0.852	0.798	0.900	1.019	0.959	0.984	0.987	1.022	1.113	esdK7
LSR2117+7345	0.798	0.289	0.610	0.214	0.849	0.516	0.590	0.717	3.624	M6.0V
LSR2122+3656	0.430	0.304	0.463	0.807	0.951	1.055	0.999	1.026	1.415	esdM5.0
LSR2124+4003	0.000	0.359	0.710	0.282	0.841	0.561	0.575	0.707	4.122	M6.5V
LSR2132+4754	0.831	0.413	0.690	0.412	0.909	0.684	0.786	0.892	2.133	M4.0V
LSR2146+5147	0.752	0.603	0.777	0.860	0.964	0.928	0.928	1.032	1.240	sdM1.0
LSR2158+6117	0.779	0.269	0.575	0.209	0.845	0.543	0.616	0.730	3.610	M6.0V
LSR2205+5353	0.721	0.612	0.782	0.950	0.991	1.019	0.973	1.029	1.199	esdM1.0
LSR2205+5807	0.780	0.630	0.745	0.867	0.983	1.025	0.920	1.058	1.607	sdM1.0
LSR2251+4706	0.740	0.229	0.535	0.154	0.835	0.489	0.568	0.662	4.601	M6.5V
LSR2311+5032	0.836	0.366	0.666	0.335	0.898	0.617	0.750	0.792	2.850	M4.5V
LSR2311+5103	1.064	0.258	0.628	0.160	0.811	0.463	0.468	0.604	6.292	M7.5V
LSR2321+4704	0.797	0.535	0.720	0.858	0.945	1.043	0.973	0.993	1.323	esdM2.0

Table 4. Estimated distances and kinematics

Star	Sp. type ¹	d(pc) ²	U (km s ⁻¹) ³	V (km s ⁻¹) ³	W (km s ⁻¹) ³
LSR0011+5908	M5.5 V	12±4	0±30	100±40	-70±20
LSR0014+6546	sdM4.5	40±20	-90±80	-220±60	30±20
LSR0020+5526	esdM2.5	70±35	-120±70	-160±60	90±40
LSR0124+6819	M7.0 V	11±3	-20±20	-30±20	-20±10
LSR0134+6459	M5.5 V	18±6	-70±30	-50±30	30±10
LSR0155+3758	M5.0 V	20±6	20±30	-80±30	-20±20
LSR0157+5308	sdM3.5	45±22	-90±50	-120±50	20±10
LSR0200+5530	M5.5 V	90±30	-120±60	-200±60	-20±10
LSR0212+7012	M5.0 V	40±13	-100±40	-80±30	70±20
LSR0258+5354	sdK7	250±100	-500±160	-430±200	-120±40
LSR0310+6634	DC10	60±30	-170±80	-170±80	-10±10
LSR0316+3132	M5.0 V	30±10	-130±30	-70±30	-70±10
LSR0340+5124	M5.5 V	18±6	-20±30	-80±30	-40±10
LSR0342+5527	sdM0.0	150±75	-270±100	-230±140	-120±60
LSR0354+3333	M6.0 V	20±6	-90±30	-60±20	-50±10
LSR0358+8111	sdM1.5	200±100	-400±200	-330±170	-100±40
LSR0400+5417	(e)sdK7	375±180	-580±340	-1220±550	-140±60
...	...	(150±75)	(-160±140)	(-540±230)	(-60±30)
LSR0401+5131	DC8	26±13	-60±20	-90±40	-50±20
LSR0419+4233	M8.5 Ve	10±3	-60±30	-60±20	-40±10
LSR0455+0244	M5.5 V	28±9	-50±30	-110±30	10±20
LSR0455+5252	M8.0 Ve	20±6	-10±30	-60±20	-60±20
LSR0505+3043	esdM3.5	70±35	-250±40	-340±180	-60±20
LSR0505+6633	sdM4.5	70±35	-50±60	-200±80	-60±20
LSR0515+5911	M7.0 V	14±4	10±40	-80±20	-50±10
LSR0519+4213	esdM3.5	55±27	-200±40	-340±130	110±70
LSR0521+3425	M5.0 V	32±10	-80±30	-70±20	-10±10
LSR0522+3814	esdM3.0	45±22	30±40	-360±170	-130±60
LSR0524+3358	sdM1.5	250±150	110±60	-640±370	80±50
LSR0527+3009	M5.0 V	40±13	-10±30	-30±10	-120±40
LSR0533+3837	sdM2.0	150±75	100±40	-410±190	70±40
LSR0539+4038	M8.0 Ve	10±3	-30±30	-50±20	0±10
LSR0541+3959	DA8	35±17	-30±30	-90±40	0±10
LSR0549+2329	DC8	40±20	10±10	-250±120	70±40
LSR0556+1144	M5.5 V	10±3	-160±30	-70±10	-10±10
LSR0609+2319	sdM5.0	45±22	60±30	-220±100	70±40
LSR0618+1614	sdM2.0	85±42	-10±40	-270±120	-70±30
LSR0621+3652	esdK7	80±40	-280±30	-290±150	-90±60
LSR0627+0616	esdM1.5	80±40	260±80	-260±160	-170±90
LSR0628+0529	M7.0 V	16±5	-90±30	-90±20	0±10
LSR0646+3212	M5.5 V	60±20	-150±80	-170±50	70±20
LSR0702+2154	M5.5 V	16±5	-10±30	-60±20	10±10
LSR0705+0506	sdM3.5	90±45	10±70	-240±100	-20±10
LSR0721+3714	M5.5 Ve	26±8	-90±30	-30±10	-50±20
LSR0731+0729	M5.0 V	24±8	-120±40	-120±30	-10±20
LSR0803+1547	sdM0.0	275±125	420±140	-540±270	-40±20
LSR1722+1004	M4.0 V	70±23	130±50	-200±70	-60±20
LSR1755+1648	sdM3.5	28±14	10±30	0±30	-140±60
LSR1757+0015	sdM4.5	75±37	90±50	-150±80	-80±40

Table 4—Continued

Star	Sp. type ¹	d(pc) ²	U (km s ⁻¹) ³	V (km s ⁻¹) ³	W (km s ⁻¹) ³
LSR1758+1417	DA10	18±9	30±20	-70±30	30±20
LSR1802+0028	esdM1.5	180±90	-220±110	-640±200	-70±20
LSR1806+1141	M4.0 V	45±15	70±40	-80±40	-40±20
LSR1808+1134	M5.0 V	18±6	20±30	-40±30	10±10
LSR1809-0219	M4.5 V	22±7	50±40	-30±20	-30±10
LSR1809-0247	M5.0 V	26±8	-30±40	-150±40	0±10
LSR1817+1328	DA10	15±7	20±40	-90±40	-20±10
LSR1820-0031	sdM2.0	85±42	100±60	-200±100	-40±20
LSR1833+2219	M5.0 V	26±8	60±20	-10±30	0±10
LSR1835+3259	M9.0 Ve	6±2	0±20	-20±30	-20±10
LSR1836+1040	esdM0.5	100±50	170±150	-430±170	-30±10
LSR1841+2421	M6.0 V	22±7	70±30	-20±30	-20±10
LSR1843+0507	M5.5 V	38±12	-10±30	-100±30	60±20
LSR1844+0947	(sd)M2.0V	250±125	280±190	-500±220	160±90
...	...	(100±50)	(70±80)	(-240±90)	(60±40)
LSR1851+2641	M6.0 Ve	20±6	-60±20	-40±30	-10±10
LSR1859+0156	M4.5 V	36±12	-60±30	-100±30	-110±30
LSR1914+2825A	sdM0.0	200±110	390±240	-320±140	30±30
LSR1914+2825B	sdM1.5	160±100	280±210	-290±120	-130±60
LSR1918+1728	esdM3.0	125±62	170±140	-350±110	-110±50
LSR1919+1438	M5.0 V	22±7	-40±30	-10±30	-60±20
LSR1922+4605	sdM0.0	200±90	500±230	-140±60	0±10
LSR1927+6802	M6.5 V	22±7	40±20	-20±40	10±20
LSR1928-0200A	M3.5 V	85±27	100±70	-340±90	-70±20
LSR1928-0200B	M5.5 V	65±22	70±60	-270±70	-50±20
LSR1933-0138	M3.0 V	50±16	-140±30	-170±30	-180±60
LSR1943+0941	M5.5 V	26±8	40±30	-50±30	0±10
LSR1945+4650A	DA9	30±15	70±40	-20±10	20±10
LSR1945+4650B	DC10	60±30	150±80	-40±10	50±30
LSR1946+0937	DA9	40±20	-40±40	-170±40	-50±30
LSR1946+0942	M3.5 V	90±30	30±50	-240±50	-130±50
LSR1956+4428	esdM0.5	75±37	280±150	-200±40	-10±10
LSR2000+0404	M5.5 V	22±7	0±30	0±30	-60±20
LSR2000+3057	M6.0 Ve	16±5	-100±30	20±40	20±10
LSR2005+0835	sdK5	275±100	520±210	-520±180	-170±60
LSR2009+5659	sdM2.0	55±27	-220±110	-130±40	-30±10
LSR2010+3938	(sd)M1.5V	225±100	390±220	-300±60	-320±150
...	...	(100±50)	(140±100)	(-250±40)	(-150±70)
LSR2013+0417	sdK7	175±87	270±220	-580±200	-100±80
LSR2017+0623	M5.0 V	40±13	80±40	-70±40	-60±20
LSR2036+5059	sdM7.5	18±9	-50±20	-130±30	-100±40
LSR2044+1339	M5.0 Ve	16±5	-50±20	0±30	0±10
LSR2050+7740	DC11	45±22	-110±50	-50±20	10±10
LSR2059+5517	DC11	25±12	-70±30	-10±10	0±10
LSR2107+3600	M4.5 V	60±20	170±70	-160±40	40±10
LSR2115+3804	esdK7	100±50	-250±110	-110±40	90±40
LSR2117+7345	M6.0 V	20±6	-100±20	30±40	10±10
LSR2122+3656	esdM5.0	45±22	-180±80	-90±40	-50±30
LSR2124+4003	M6.5 V	7±2	-40±10	-60±30	0±10

Table 4—Continued

Star	Sp. type ¹	d(pc) ²	U (km s ⁻¹) ³	V (km s ⁻¹) ³	W (km s ⁻¹) ³
LSR2132+4754	M4.0 V	45±15	-125±40	-70±40	20±10
LSR2146+5147	sdM1.0	200±100	-540±290	-280±50	+10±10
LSR2158+6117	M6.0 V	14±4	-40±20	-80±40	-40±10
LSR2205+5353	sdM1.0	100±50	270±120	-160±50	10±10
LSR2205+5807	esdM1.0	70±35	-80±50	-150±40	-160±70
LSR2251+4706	M6.5 V	35±11	-90±30	-130±40	0±10
LSR2311+5032	M4.5 V	30±9	-90±30	-60±30	-20±10
LSR2311+5103	M7.5 V	26±8	50±20	10±40	0±10
LSR2321+4704	esdM2.0	85±42	-220±140	-300±50	40±10

¹Spectral class and subtype based on spectroscopy. Parenthesis indicate possible change in spectral class that would lower the star’s components of velocity to more consistent values. The modified values are given in parenthesis one line below.

²Spectroscopic distance estimate.

³UVW components of the velocity relative to the local standard of rest, calculated from the radial velocities, proper motions, and estimated distances.

Table 5. Blackbody temperature fits for the white dwarfs

Star	$T_{blackbody}$	Spectral type
LSR0310+6634	5000	DC10
LSR0401+5131	6500	DC8
LSR0541+3959	6000	DA8
LSR0549+2329	6000	DC8
LSR1758+1417	5250	DA10
LSR1817+1328	5000	DA10
LSR1945+4650A	5750	DA9
LSR1945+4650B	5000	DC10
LSR1946+0937	5750	DA9
LSR2050+7740	4750	DC11
LSR2059+5517	4750	DC11

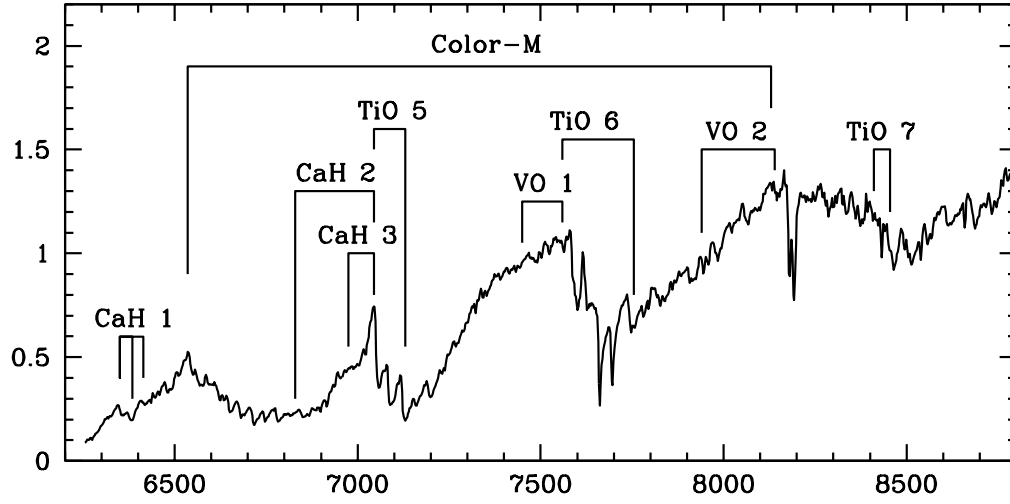


Fig. 1.— Illustration of the different spectral indices cited in this paper, as defined in Table 1, here shown with the spectrum of the star LSR1809-0247 (M5.0 V). The indices measure the strengths of all the most prominent molecular features in the 6000Å-9000Å range.

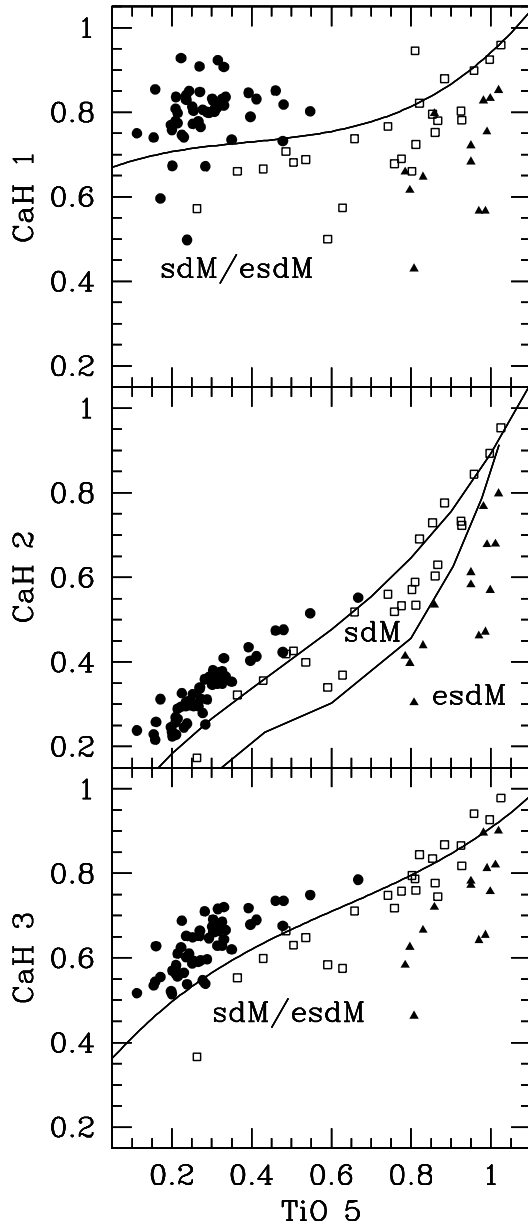


Fig. 2.— Separation of the high proper motion red dwarfs into three metallicity classes (dwarfs dM, subdwarfs sdM, extreme subdwarfs esdM) based on the ratio of the CaH spectral indices with the TiO5 spectral index. This classification scheme is based on the criteria defined by G97. We use the CaH2/TiO5 ratio as the main criterion. The three classes show up well separated by the CaH3/TiO5 ratio. The CaH1/TiO5 ratio, on the other hand, does not discriminate as well between the dM and sdM classes; the shorter dynamic range of the CaH1 index makes classification with the CaH1/TiO5 ratio more sensitive to measurement errors.

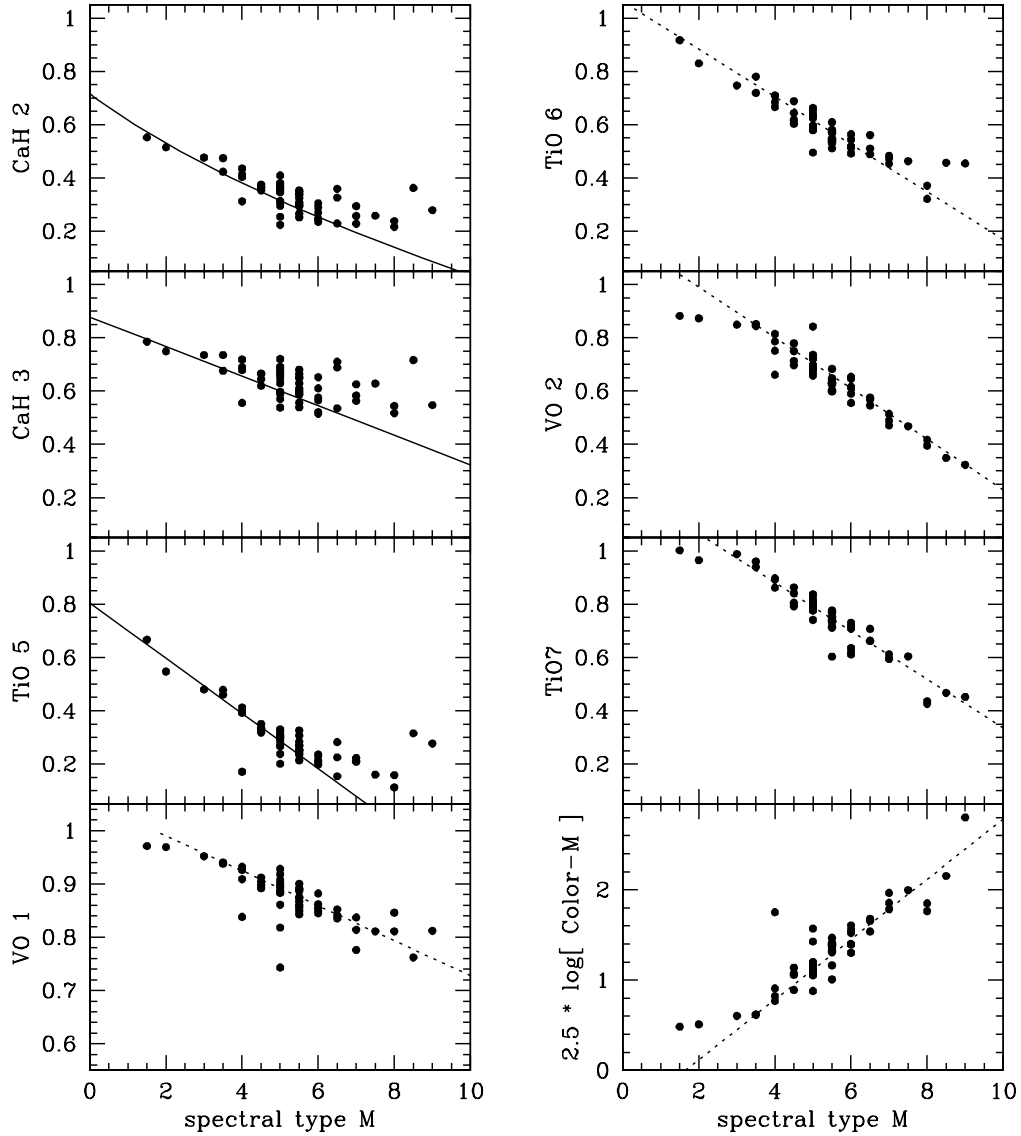


Fig. 3.— Correlation between spectral type and the different spectral indices, for the 54 M dwarf stars classified in this paper. The relationships determined by G97 for the CaH2, CaH3, and TiO5 indices are plotted in continuous lines. Our new relationships for the other indices are plotted as dotted lines. Classification of early-type M dwarfs is more reliable when the blueward indices (CaH2, TiO5) are used, while late-type M dwarfs are better classified with our newly defined redward indices (VO 2, TiO7). Negative values correspond to K dwarf spectra, with $-2 \rightarrow K5V$ and $-1 \rightarrow K7V$.

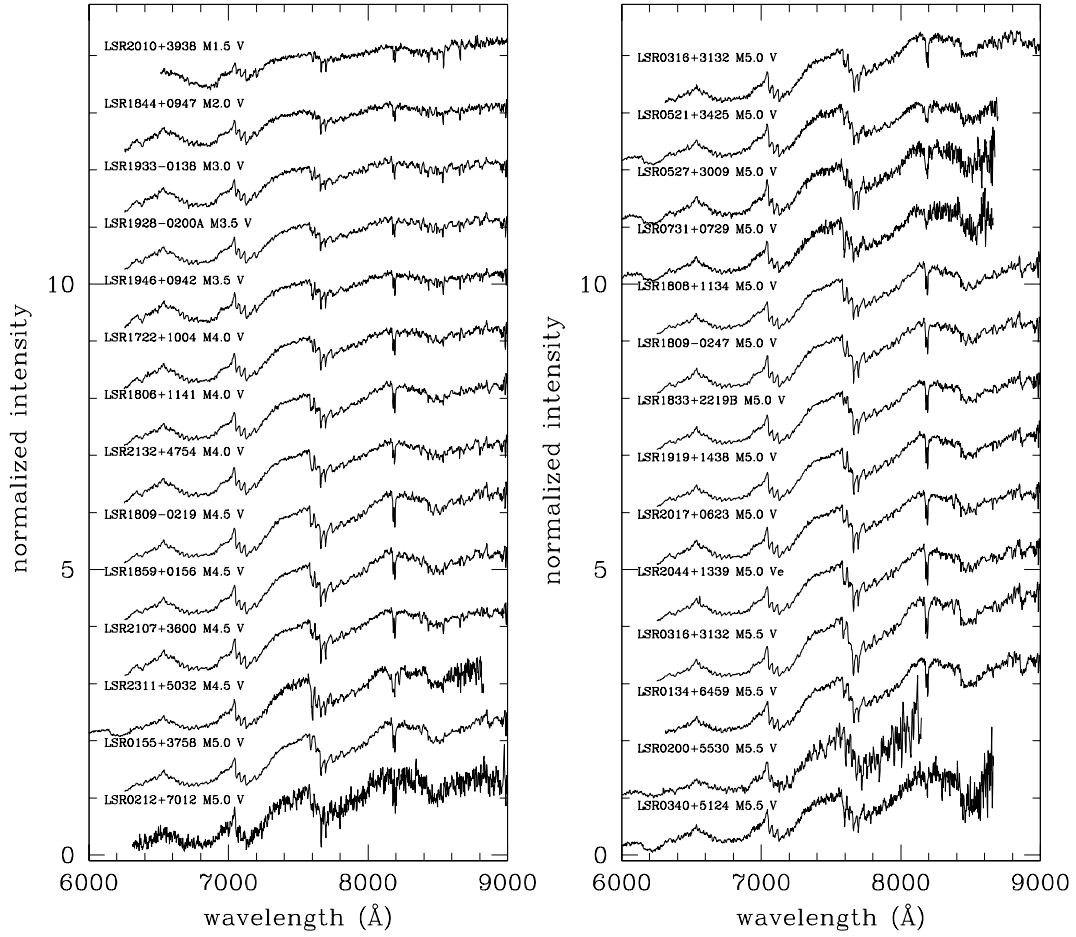


Fig. 4.— Spectral sequence for M dwarf stars classified in this paper. Spectra have been normalized to 1.0 at 7500Å and shifted vertically by integer values for clarity. The later-type stars are displayed on Figure 5.

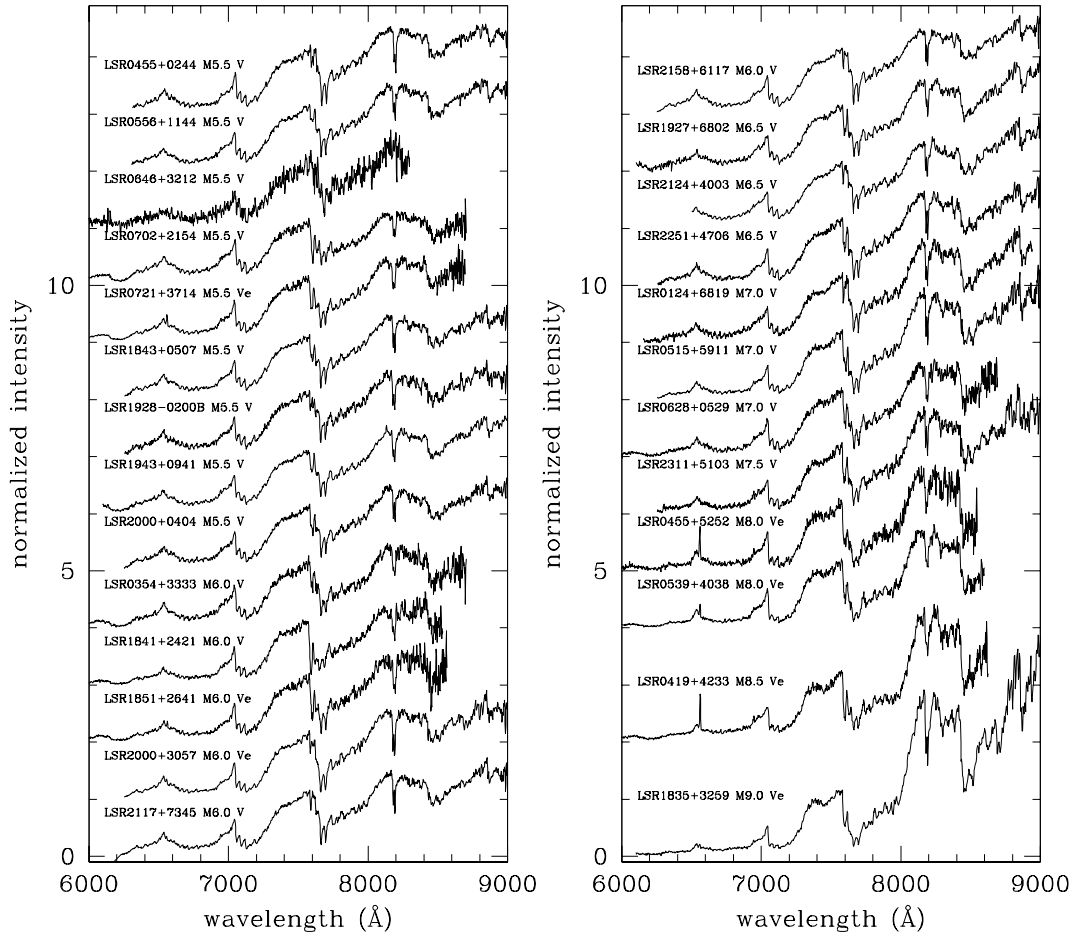


Fig. 5.— Spectral sequence for M dwarf stars classified in this paper, continued from Figure 4.

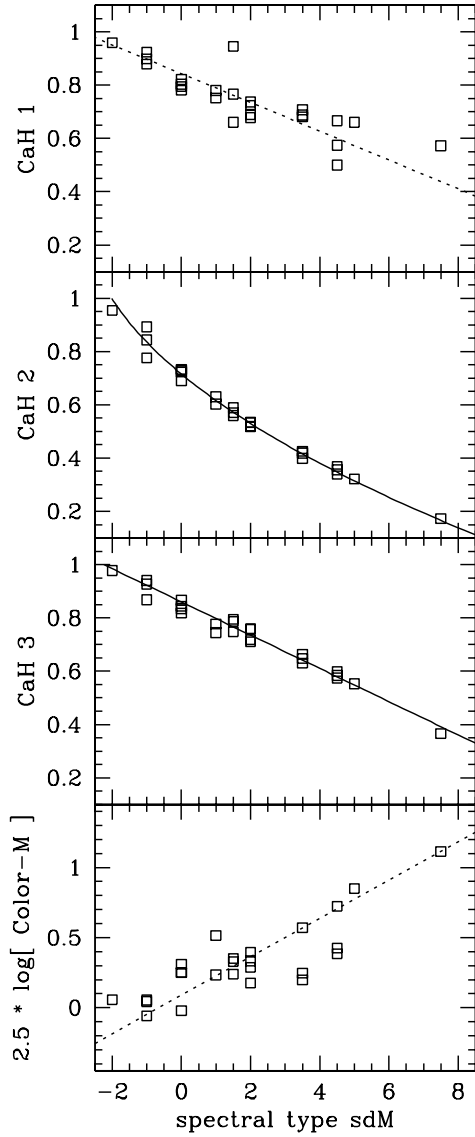


Fig. 6.— Classification of the subdwarfs based on spectral features. Classification is based of the CaH2 and CaH3 spectral indices. The relationships determined by G97 are plotted in full lines. Values of the CaH1 index and of the Color-M index are plotted against spectral type for comparison. Negative values correspond to sdK dwarf spectra, with -2→sdK5 and -1→sdK7.

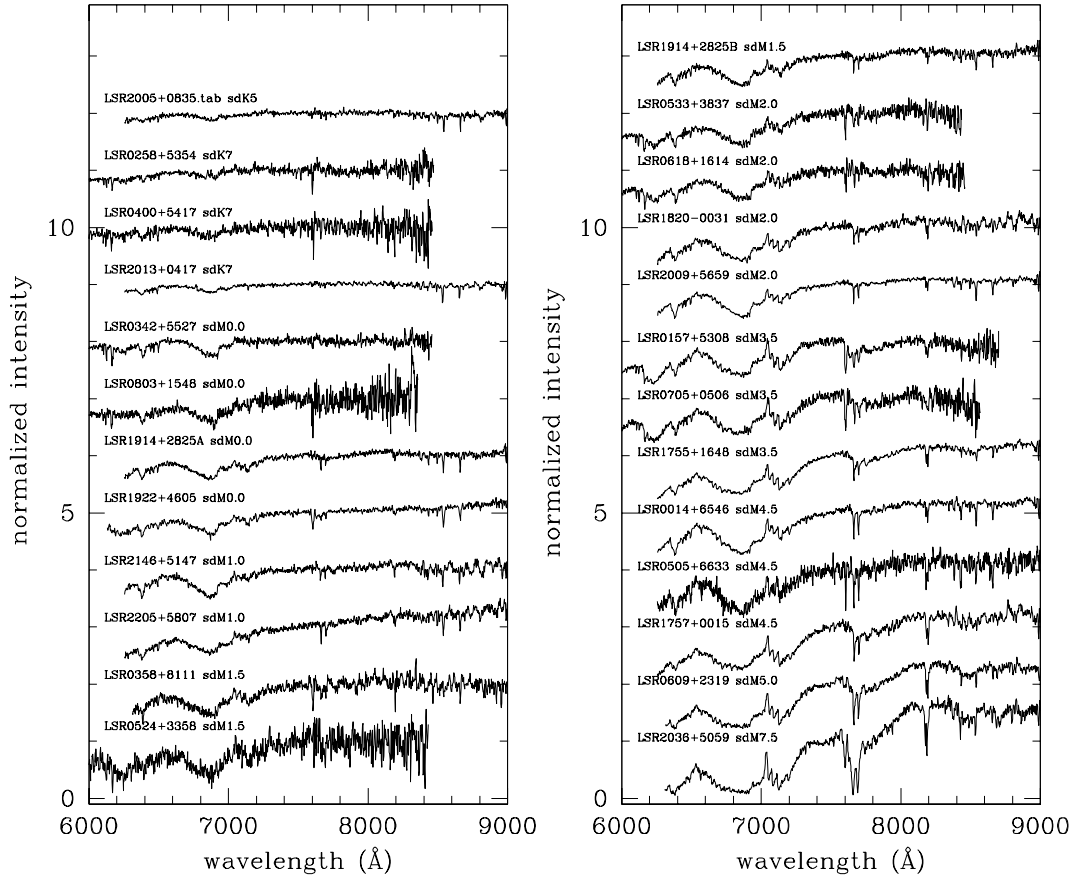


Fig. 7.— Spectral sequence for subdwarf (sdM) stars classified in this paper. Spectra have been normalized to 1.0 at 7500\AA and shifted vertically by integer values for clarity.

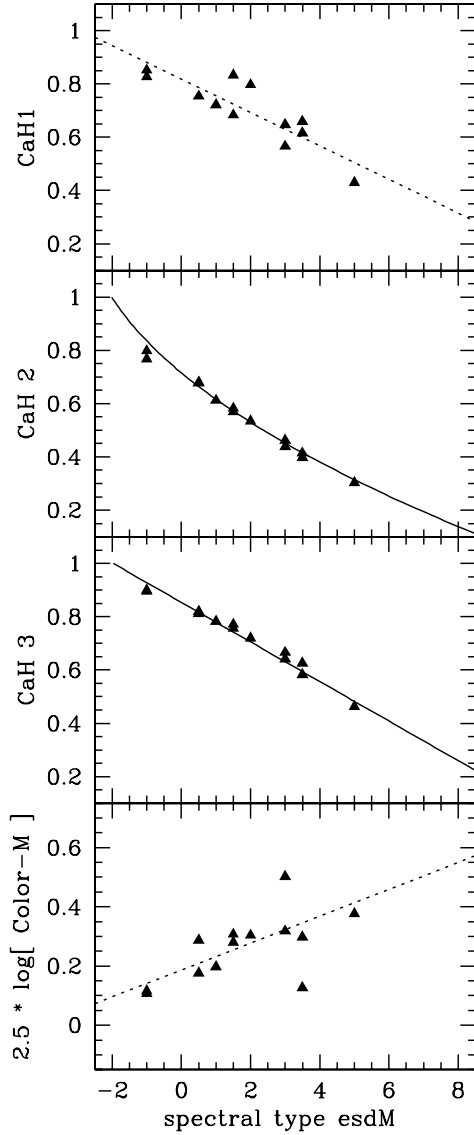


Fig. 8.— Classification of the extreme subdwarfs based on spectral features. Classification is based of the CaH2 and CaH3 spectral indices. The relationships determined by G97 are plotted in full lines. Values of the CaH1 index and of the slope of the continuum index are plotted against spectral type for comparison. Negative values correspond to esdK dwarf spectra, with $-1 \rightarrow \text{esdK7}$.

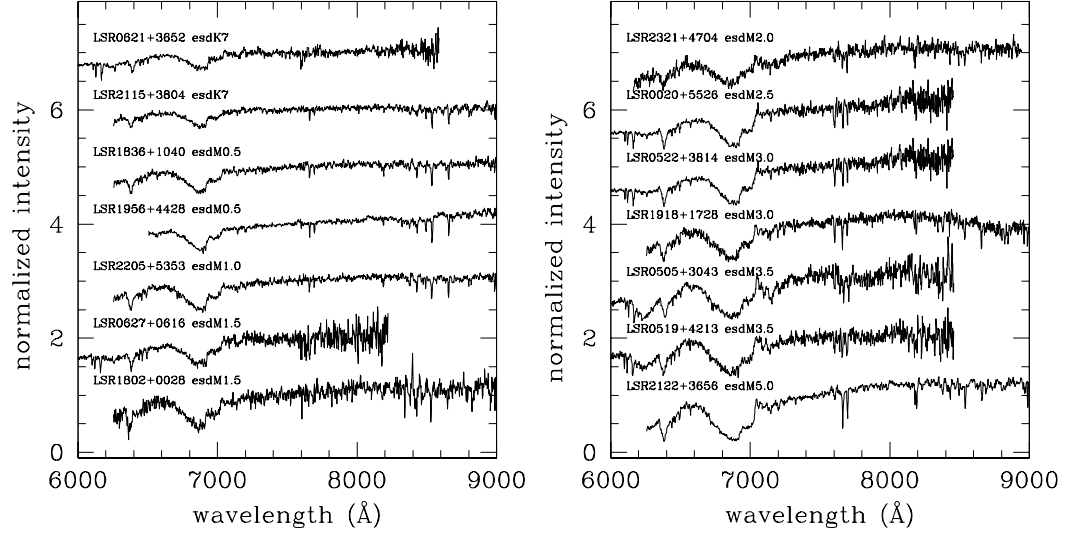


Fig. 9.— Spectral sequence for extreme subdwarf (esdM) stars classified in this paper. Spectra have been normalized to 1.0 at 7500\AA and shifted vertically by integer values for clarity. Several spectra are very noisy because we used a spectroscopic setup optimized for the observation of red dwarfs.

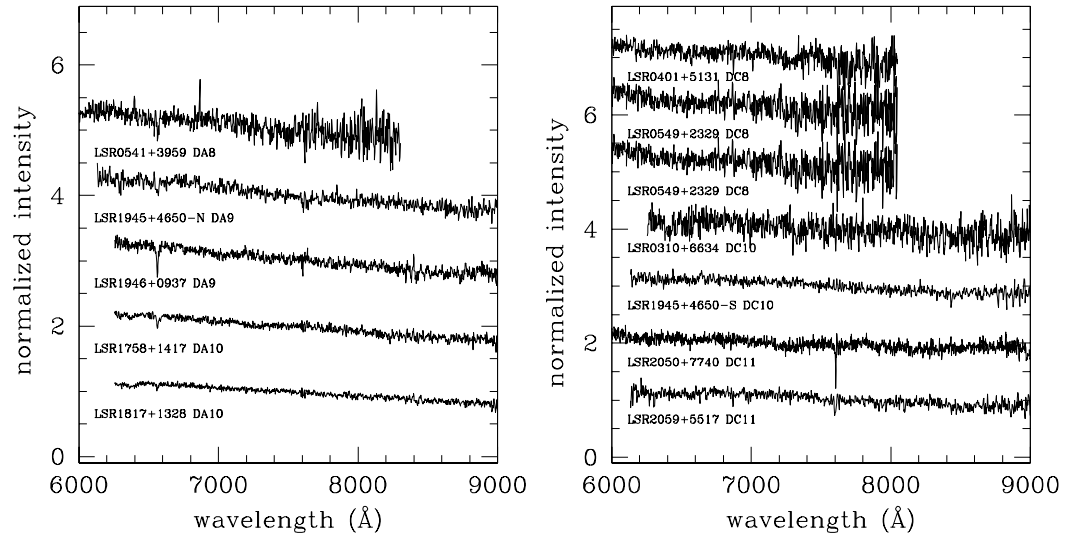


Fig. 10.— Spectra of the white dwarfs found in the sample of new high proper motion stars. All the spectra are normalized to 1.0 at 7500\AA , and shifted by integer values on the vertical scale for clarity.

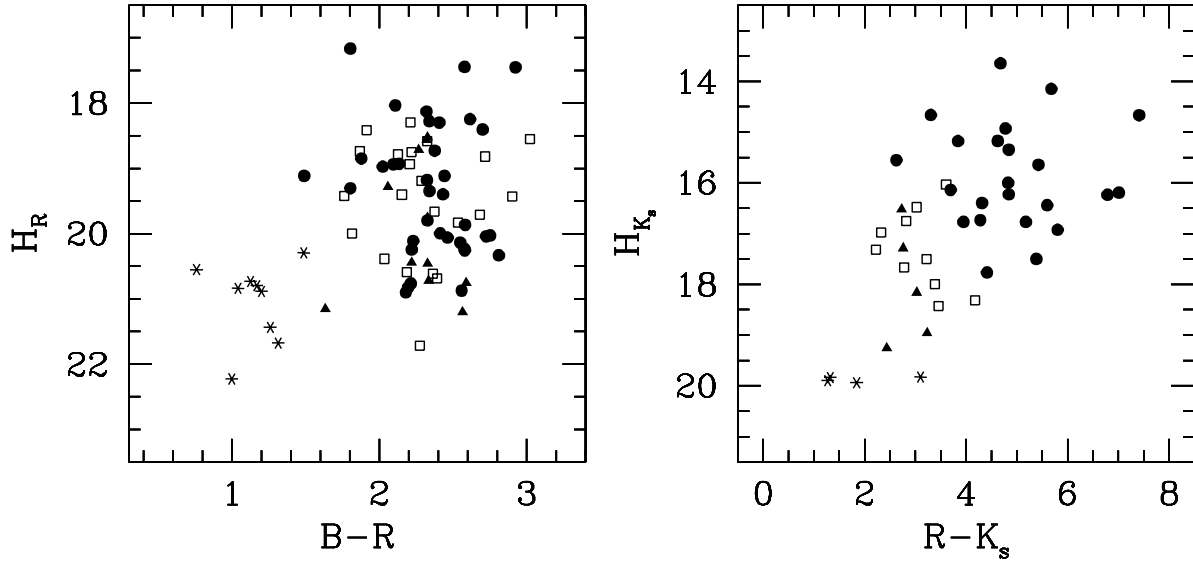


Fig. 11.— Reduced proper motion diagrams for the stars classified in this paper. The reduced proper motion terms are derived from $H_R = R + \log \mu + 5$, and $H_{K_s} = K_s + \log \mu$, where μ is the proper motion of the star. Red dwarfs are represented by filled circles, subdwarfs (sdM) by open squares, extreme subdwarfs (esdM) by filled triangles, and white dwarf by asterisks.

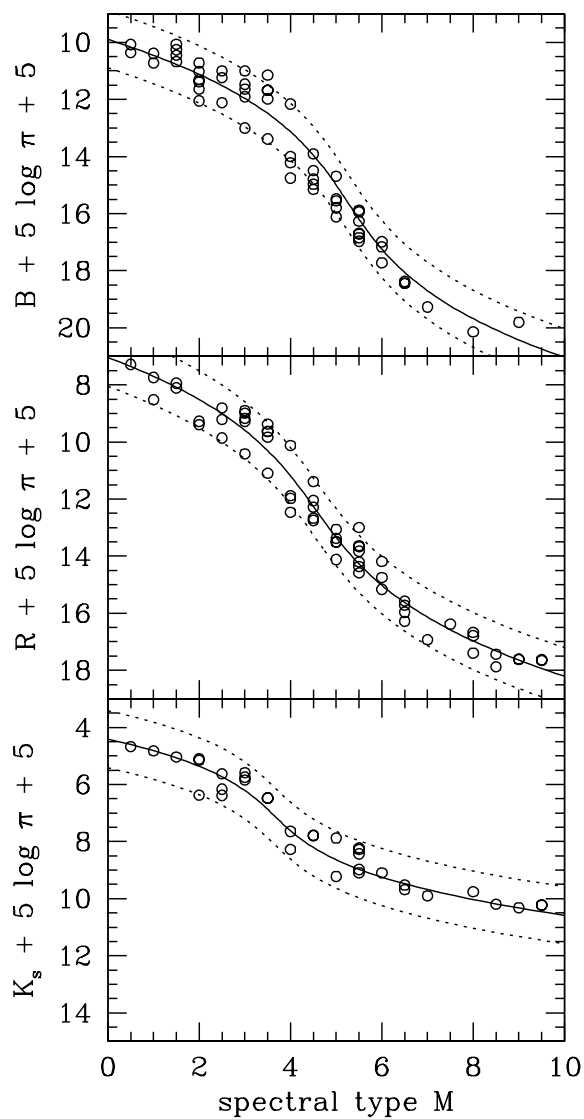


Fig. 12.— Empirical spectral-type / absolute magnitude relationship for a sample of nearby M dwarfs with assigned spectral types and measured astrometric parallaxes (π). The observed B and R magnitudes are those recorded on the IIIaJ (blue) and IIIaF (red) POSS-II plates as listed in the Second Guide Star Catalog (GSC2.2.1), the K_s magnitudes are from the 2MASS Second incremental Release. The relationships (continuous lines) are determined from third order polynomial fits. Most stars fall within 1 magnitude of the adopted relationship (dashed lines).

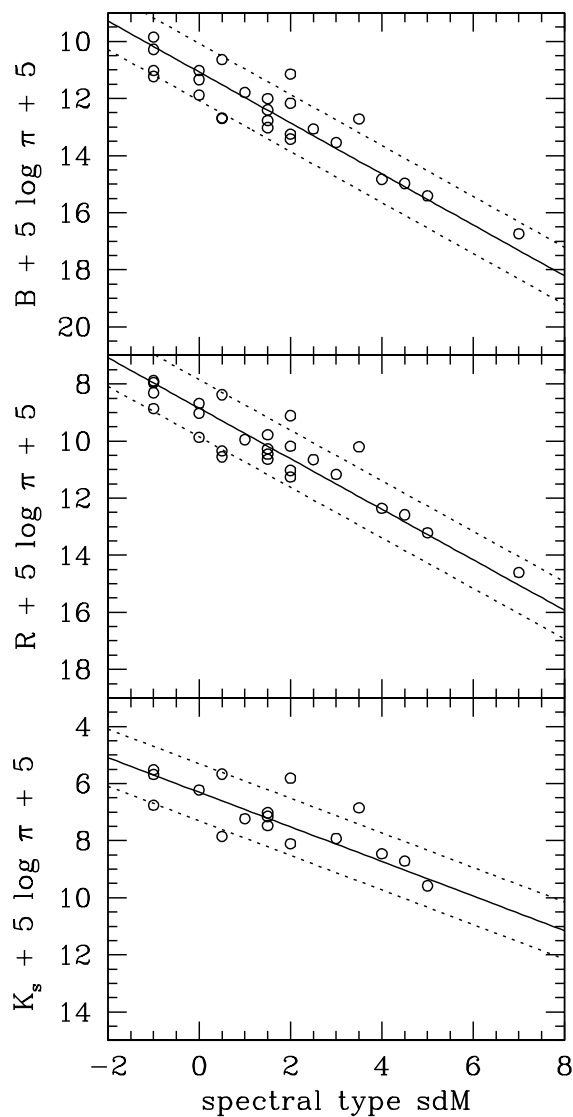


Fig. 13.— Empirical spectral-type / absolute magnitude relationship for a sample of sdM dwarfs with assigned spectral types and measured astrometric parallaxes (π). The observed B and R magnitudes are those recorded on the IIIaJ (blue) and IIIaF (red) POSS-II plates as listed in the Second Guide Star Catalog (GSC2.2.1), the K_s magnitudes are from the 2MASS Second incremental Release. The linear relationships (continuous lines) are determined from first order polynomial fits. Dashed lines mark the 1 magnitude scatter.

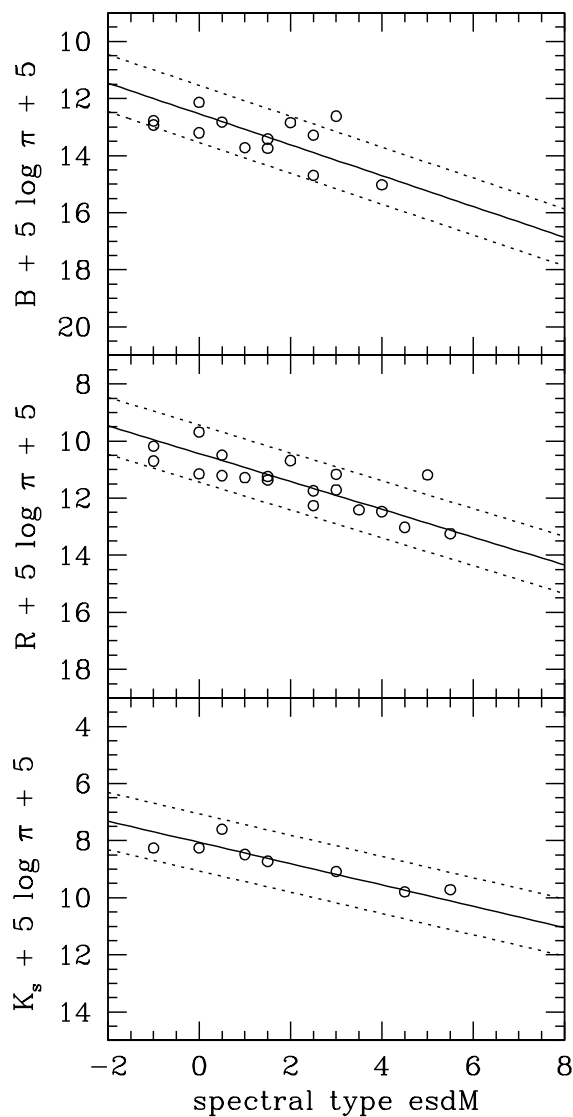


Fig. 14.— Empirical spectral-type / absolute magnitude relationship for a sample of esdM dwarfs with assigned spectral types and measured astrometric parallaxes (π). The observed B and R magnitudes are those recorded on the IIIaJ (blue) and IIIaF (red) POSS-II plates as listed in the Second Guide Star Catalog (GSC2.2.1), the K_s magnitudes are from the 2MASS Second incremental Release. The linear relationships are determined from first order polynomial fits. Dashed lines mark the 1 magnitude scatter.

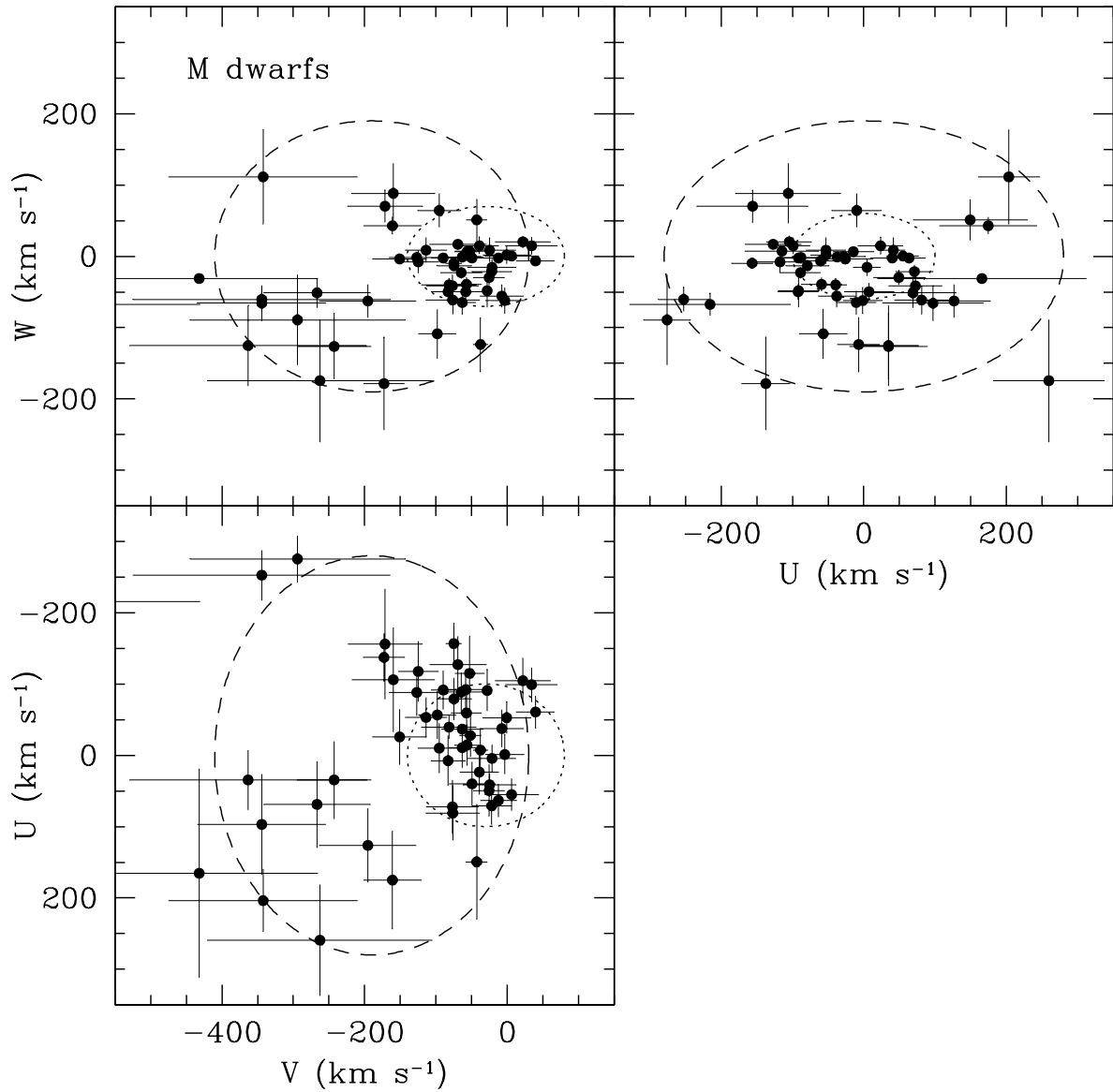


Fig. 15.— UVW velocity space distribution of the newly classified M dwarfs. The dotted line shows the 2σ dispersion of local disk stars and the dashed line the 2σ dispersion of local halo stars, based on observations compiled by Chiba & Beers (2000). A significant number of M dwarfs have kinematics that are more consistent with the halo than with the disk.

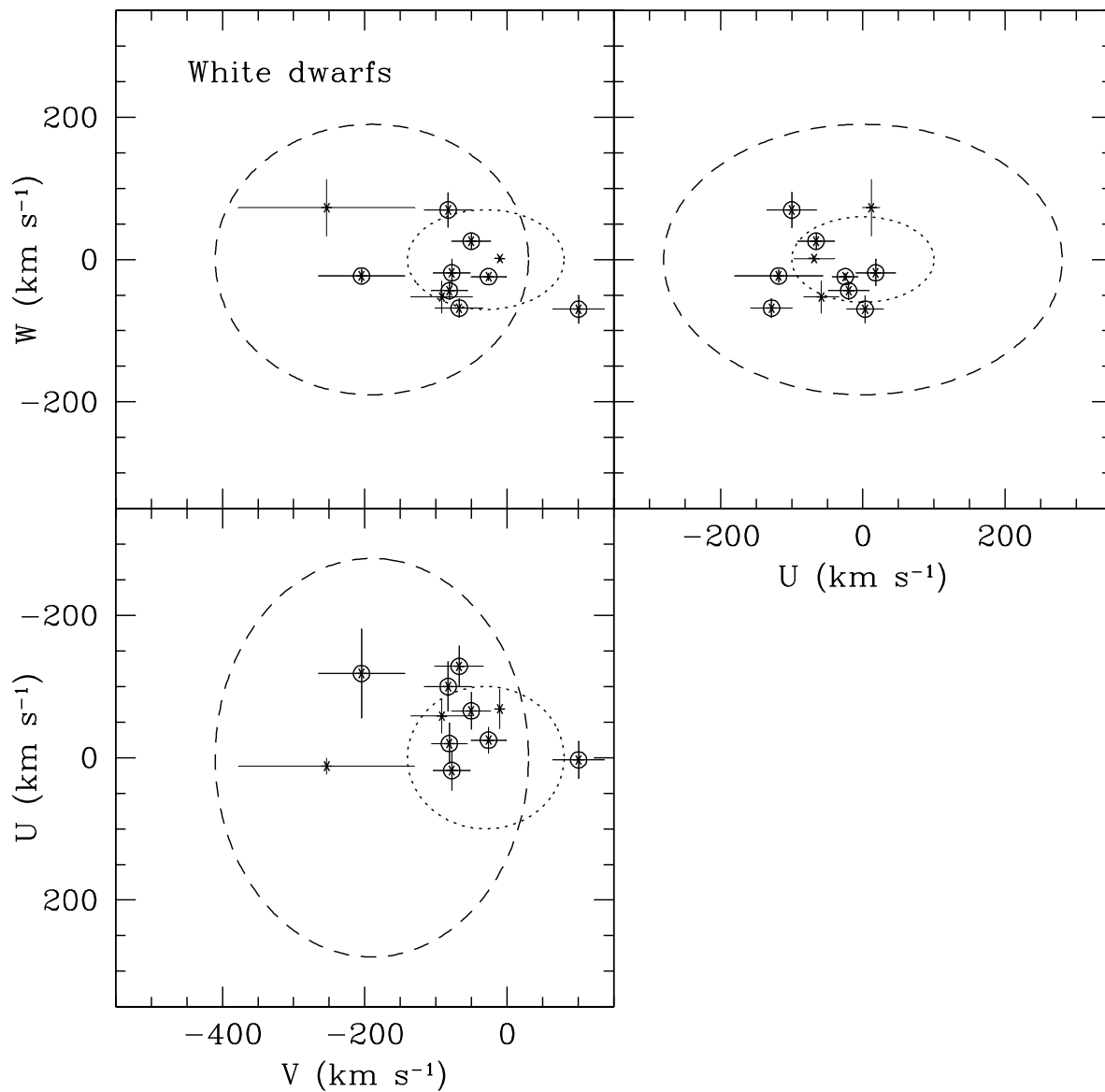


Fig. 16.— Same as in Figure 15, but for the new white dwarfs identified in our sample. Circled asterisks indicate those stars for which we do not have radial velocities; heliocentric radial velocity $HRV=0$ is then assumed. The distribution appears to be very similar to that of the M dwarfs (see Fig.15) with a few white dwarfs falling in the region more typical for local halo stars.

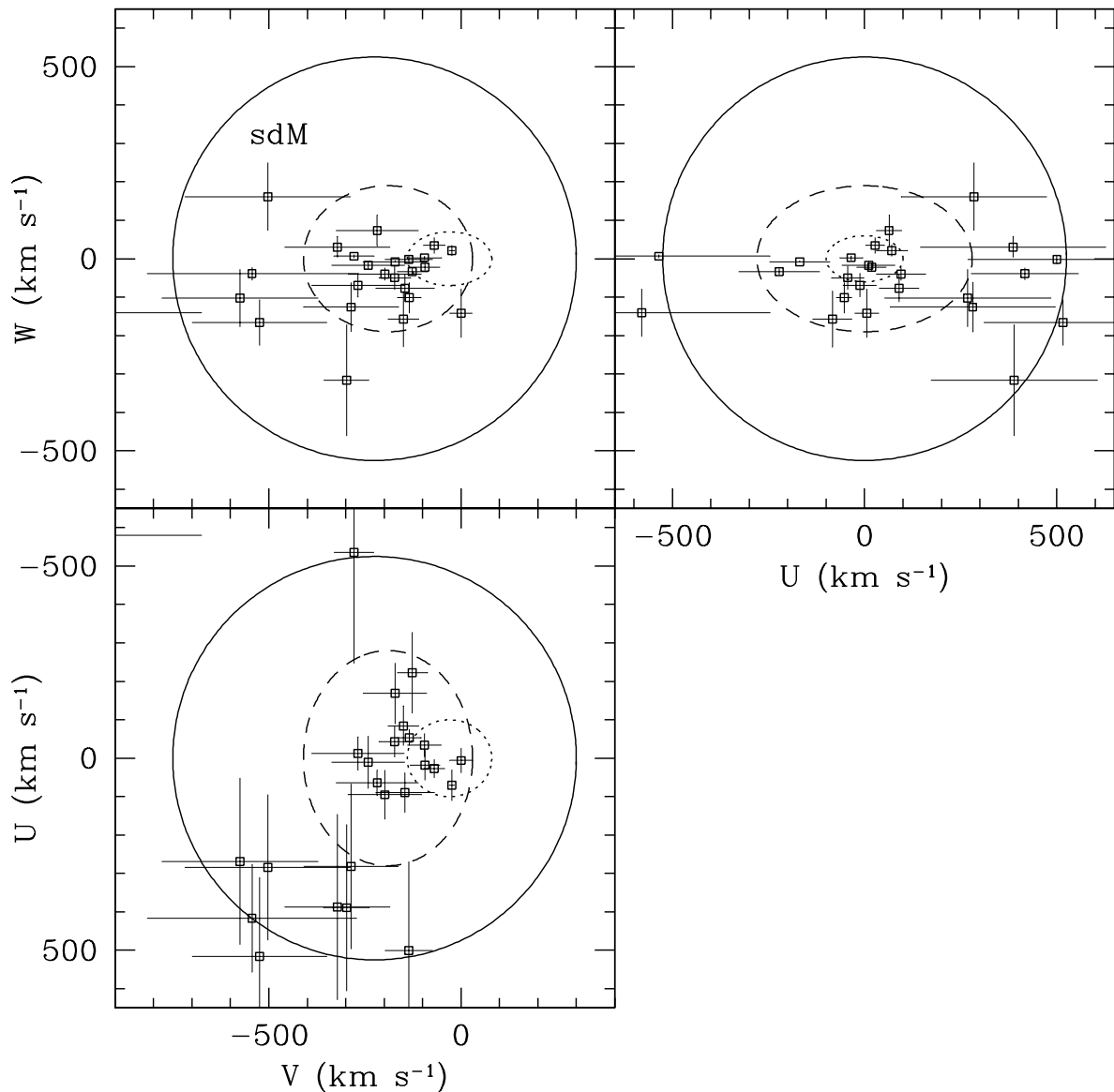


Fig. 17.— UVW velocity space distribution of the newly classified subdwarfs. The dotted line shows the 2σ dispersion of local disk stars and the dashed line the 2σ dispersion of local halo stars, based on observations compiled by Chiba & Beers (2000). The full line shows the limits within which stars are gravitationally bound to the Galaxy, as calculated from the Galactic model of Dauphole & Colin (1995). The distribution is significantly different from that of the M dwarfs and white dwarfs (see Figs.15-16), and is clearly consistent with a kinematics similar to halo stars.

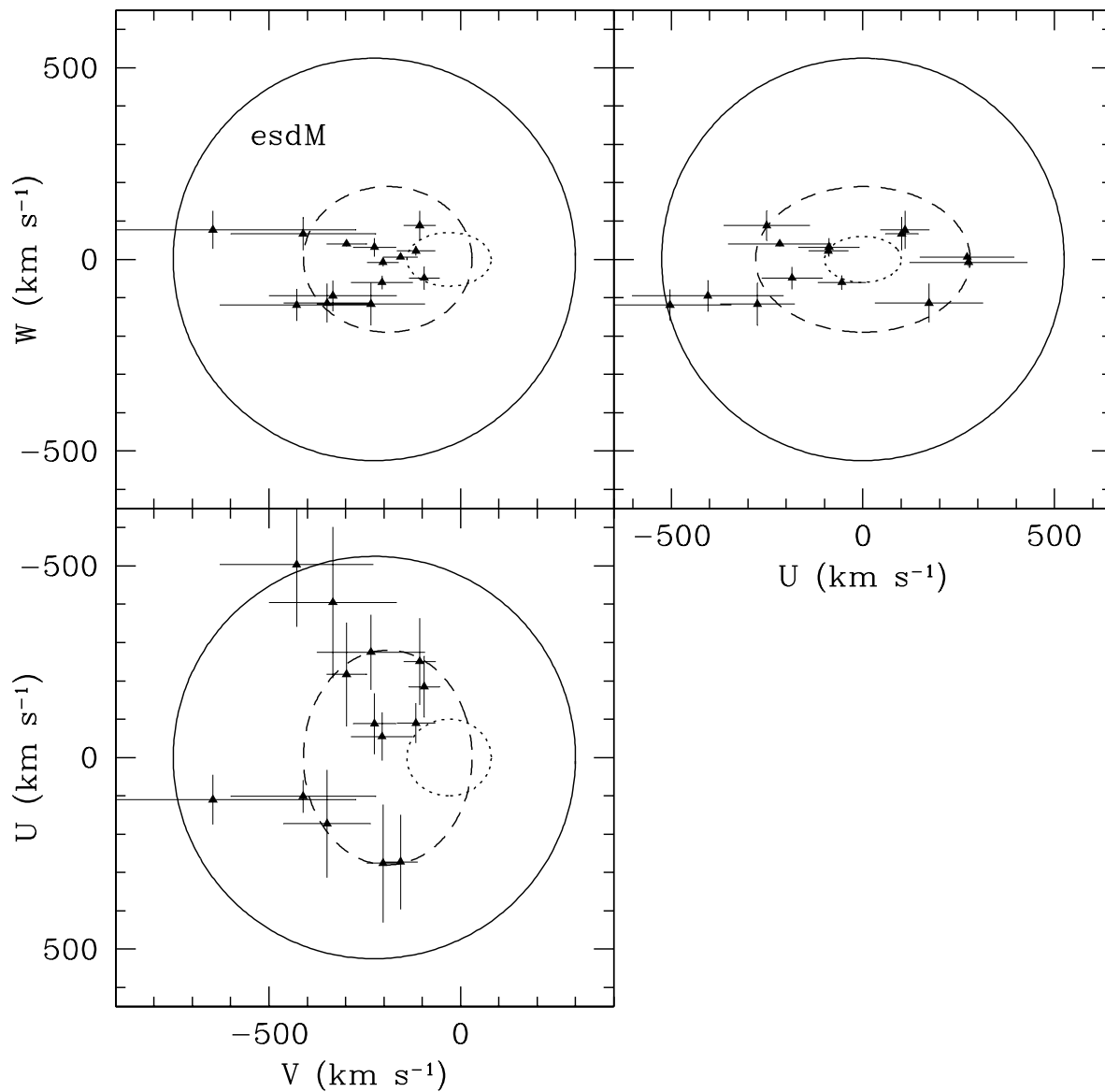


Fig. 18.— Same as in Figure 17, but for the extreme subdwarfs in our sample. Again, the distribution of esdK/esdM stars is significantly different from that of the M dwarfs and white dwarfs (see Figs.15-16), and is clearly consistent with a kinematics similar to halo stars. The velocity space distribution of extreme subdwarfs does not, however, appear to be different from that of the subdwarfs (see Fig.17).